Analytical and numerical studies of finite length plasma systems with flows

A Thesis Submitted to the
College of Graduate Studies and Research
in Partial Fulfillment of the Requirements
for the degree of Master of Science
in the Department of Physics and Engineering Physics
University of Saskatchewan
Saskatoon

By
Oleksandr Koshkarov

Permission to Use

In presenting this thesis in partial fulfilment of the requirements for a Postgraduate degree from the University of Saskatchewan, I agree that the Libraries of this University may make it freely available for inspection. I further agree that permission for copying of this thesis in any manner, in whole or in part, for scholarly purposes may be granted by the professor or professors who supervised my thesis work or, in their absence, by the Head of the Department or the Dean of the College in which my thesis work was done. It is understood that any copying or publication or use of this thesis or parts thereof for financial gain shall not be allowed without my written permission. It is also understood that due recognition shall be given to me and to the University of Saskatchewan in any scholarly use which may be made of any material in my thesis.

Requests for permission to copy or to make other use of material in this thesis in whole or part should be addressed to:

Head of the Department of Physics and Engineering Physics
Rm 163
116 Science Place
University of Saskatchewan
Saskatoon, Saskatchewan
Canada
S7N 5E2

Abstract

In many natural and laboratory conditions, plasmas are often in the non-equilibrium state due to presence of stationary flows, when one particle species (or a special group, such as group of high energy particles, i.e., beam) is moving with respect to the other plasma components. Such situations are common for a number of different plasma applications such as diagnostics with emissive plasma probes, plasma electronics devices and electric propulsion devices. The presence of plasmas flows often leads to the instabilities in such systems and subsequent development of large amplitude perturbations. The goal of this work is to develop physical insights and numerical tools for studies of ion sound instabilities driven by the ion flow in a system of a finite length. The ion sound waves are modified by the presence of ion beam resulting in negative and positive energy modes. The instability develops due to coupling of negative and positive energy modes mediated by reflections from the boundary. It is shown that the wave dispersion due to deviation from quasi-neutrality is crucial for the stability. In finite length system, the dispersion is characterized by the length of the system measured in units of the Debye length. The instability is studied analytically and the results are compared with direct initial value numerical simulations. The numerical tools to simulate these systems are developed based on Godunov and multiple shooting methods. The initial value simulations show the time dependent evolution from which the growth rates were determined for different parameters of the system. The results of the simulations were benchmarked against the analytical results in some limiting cases. In the pursuit of simulation efficiency, the parallelization of the code was investigated for two basic types of parallel systems: shared and distributed memory. The OpenMP and MPI library were used correspondingly.

Acknowledgements

I would like to thank my supervisor Professor Dr. Andrei Smolyakov, who has been a great teacher. Thank you for encouraging my research and for introducing me for the world of science. Your advice and help were priceless for me and crucial for my research. I would also like to thank my co-supervisor Professor Dr. Victor Ilgisonis who introduced me to the theoretical plasma physics and prepared me for the research work. You have ignited my passion for theoretical physics. I would like to thank Professor Igor Kaganovich and Dr. Dmitriy Sydorenko whose plasma PIC simulations provoked my research. I would also like to thank my committee members for comments and suggestions. I would especially like to thank my fellow graduate students at University of Saskatchewan who helped and supported me. The support of the Deans Scholarship, NSERC and Compute Canada (Westgrid) is also acknowledged with gratitude.

A special thanks to my family for their constant support and belief in me.

All of you have been a great support to me.

Thank you!

Contents

List of Tables

List of Figures

Chapter 1

Introduction

Plasma is the most common form of substance in the visible universe, but what is plasma? Plasma is an ionized gas of charged particles. Often it is called the fourth fundamental state of matter, which occurs at high temperatures when neutral atoms are ionized to form a gas of electrons and ions. Energies in excess of the ionization potential are required to achieve this state. Because of the long-range nature of the Coulomb interactions plasmas exhibit collective behavior leading to waves and fluctuations. Because of this variety of wave phenomena, plasmas have been a test-bed for many developments in nonlinear wave theory and turbulence [1]. Plasma studies are important for applications to space physics, as well as for large number of laboratory devices used for material processing, plasma electronics, electric propulsion etc.

Space and laboratory plasmas often include equilibrium flows of ions and/or electrons. Such situations occur in various plasma devices for electric propulsion, plasma diodes, plasma accelerators, plasma processing devices, and emissive probe diagnostics. Plasmas permeated by energetic beams are also a common situation in space physics and astrophysics [2]. Such plasmas represent a typical example of a non-equilibrium system prone to instabilities due to the presence of a free energy reservoir from equilibrium flows. Therefore the issue of stability properties of such plasma systems with flows is important.

This work is devoted to studies of one simple example of ion sound wave excitation when the relative velocity between electrons and ions exceeds the ion sound velocity, $v_0 > c_s$. [1,3,4]. In infinite length plasmas, the instability may occur as a result of the kinetic interaction of electrons with the ion beam (two-stream instability due to inverse Landau damping). On other hand, a number of practical plasma configurations have finite length, and it is of interest to investigate the modification/new regimes of instabilities related to the presence

of boundaries. Instabilities due to accelerated ion flows are of interest for the sheath region of plasma-material boundaries [5], plasma diodes [6, 7], double layers [8–11], and electric propulsion systems [12]. In an infinite length plasma, the equilibrium ion flow v_0 results in the Doppler shift of the ion sound waves frequency, $\omega \to \omega - kv_0$. It is shown in this work that in finite length systems, ion sound waves can be destabilized due to reflections from boundaries and the coupling with ballistic modes, $\omega = kv_0$, supported by the ion flow. This instability is different from the above noted two-stream type ion sound instability where the kinetic resonances are important.

The Pierce plasma diode [13] is a well studied case of the instability driven by electron flow in a finite length system. Various extensions of the instabilities in Pierce-like plasma systems and related numerical and experimental studies have been discussed in the literature [6, 14–18]. It is shown in this work that the problem of the ion sound waves in a system with boundaries, in a special limit of strong dispersion, is formally reduced to the Pierce-like equations. In our model we consider only fluid (hydrodynamic) effects, ions are assumed to be cold (to avoid Landau damping) and have an uniform velocity with respect to the electron component. Electrons are assumed to be in Boltzmann equilibrium (electron inertia effects are neglected). We employ analytical and numerical methods to analyze the structure of unstable eigen-modes, to determine the dispersion relations and conditions for the instability, and to find the frequencies and growth rates of the unstable modes.

1.1 Ion sound oscillations

Ion sound oscillations are one of the simplest eigen-modes of finite temperature plasmas. The ion sound wave is longitudinal oscillations of ions and electrons with properties similar to sound waves in neutral gases. The restoring force is created by the electron compressibility (pressure) and is transferred to ions via the electric field. The inertia is provided by ions. These waves exist both in unmagnetized and magnetized plasmas. In Hall plasmas (when ions are not magnetized) ion sound waves may propagate in any direction except exactly perpendicular to the magnetic field. The simplest model of ion sound waves is obtained from a hydrodynamic approach. We assume a fully ionized plasma of protons and electrons,

neglecting magnetic field effects. The relevant equations are

$$\frac{\partial n_\alpha}{\partial t} + \nabla \cdot (n_\alpha \mathbf{v}_\alpha) = 0, \tag{1.1a}$$

$$m_\alpha n_\alpha \left(\frac{\partial}{\partial t} + \mathbf{v}_\alpha \cdot \nabla \right) \mathbf{v}_\alpha = -\nabla p_\alpha - e_\alpha n_\alpha \nabla \phi, \tag{1.1b}$$

$$\nabla^2 \phi = -4\pi \sum_\alpha e_\alpha n_\alpha, \tag{1.1c}$$

where Eqs. (1.1a,b) are continuity and momentum balance equations, the last Eq. (1.1c) is a Poisson equation, α - a species index (i or e), n - particle density, v - velocity, p - pressure, e - charge , ϕ - electrostatic potential.

Since electrons are much lighter than ions and the wave frequency is not too high (in comparison with plasma frequency), we could neglect electron mass in the momentum balance equation, resulting in

$$\frac{\nabla n_e}{n_e} = \frac{e}{T_e} \nabla \phi \Rightarrow n_e = n_0 \exp\left(\frac{e\phi}{T_e} \right), \tag{1.2}$$

where n_{0e} is an electron density in equilibrium.

We will consider the situation when the ion temperature is much smaller than that of electrons, $T_e \gg T_i$. This is often the case for laboratory collisionless plasma because electrons have much larger mobility than ions. Moreover, it can be shown from the kinetic theory that ion sound is subject to strong Landau damping when the ion temperature is of the order of the electron temperature ($T_i \sim T_e$) [19]. So, imposing $T_i = 0$ ($p_i = 0$) for ions one has

$$\frac{\partial n_i}{\partial t} + \nabla \cdot (n_i \mathbf{v}_i) = 0, \tag{1.3a}$$

$$m_i \left(\frac{\partial}{\partial t} + \mathbf{v}_i \cdot \nabla \right) \mathbf{v}_i + e \nabla \phi = 0. \tag{1.3b}$$

The electron and ion equations are closed with the Poisson equation

$$\nabla^2 \phi = -4\pi e \left(n_i - n_e \right). \tag{1.4a}$$

We study linear wave oscillations for small deviations from given stationary equilibrium. Thus, we will expand all variables around the equilibrium

$$X(\mathbf{r},t) = X_0(\mathbf{r}) + \widetilde{X}(\mathbf{r},t), \tag{1.5}$$

where X_0 is equilibrium value, $\widetilde{X}$ - perturbation (below, all variables without index are perturbed).

Considering the case without equilibrium flow ($\mathbf{v}_0 = 0$) and $n_{0e} = n_{0i} = n_0$, the linearized system takes the form

$$\frac{\partial n_i}{\partial t} + n_0 \nabla \cdot \mathbf{v}_i = 0, \tag{1.6a}$$

$$m_i \frac{\partial \mathbf{v}_i}{\partial t} + e\nabla\phi = 0, \tag{1.6b}$$

$$n_e = \frac{n_0 e}{T_e}\phi, \tag{1.6c}$$

$$\nabla^2\phi = -4\pi e\left(n_i - n_e\right). \tag{1.6d}$$

Using a quasi-neutral approximation $n_i = n_e = n$, Eqs. (1.6) are simplified giving the wave equation for sound waves

$$\left(\nabla^2 - \frac{1}{c_s^2}\frac{\partial^2}{\partial t^2}\right) n = 0, \tag{1.7}$$

where $c_s^2 = T_i/m_i$ is the ion sound velocity.

To obtain the dispersion relation, we seek solution for Eqs (1.6) or (1.7) in the form: $X \sim e^{i(\mathbf{k}\cdot\mathbf{r}-\omega t)}$. The dispersion equation for quasi-neutral case then is

$$\omega^2 = k^2 c_s^2. \tag{1.8}$$

1.1.1 Dispersion of ion sound waves

To include the dispersion of the ion sound waves, we should replace quasi-neutrality condition $n_i = n_e = n$ with the Poisson equation (1.6d). In this case, the dispersion equation will be

$$\omega^2 = \frac{k^2 c_s^2}{1 + k^2 d_e^2}, \tag{1.9}$$

where $d_e^2 = T_i/4\pi e^2 n_0$ - Debye length (also known as Debye radius). The Debye length is a natural plasma parameter which describes charge separation. This effect is also known as Debye screening which means that the electric field of a charge in a plasma is screened at distances roughly exceeding the Debye length.

1.1.2 Nonlinearity and wave breaking

When the amplitude of oscillations grows to a finite value we should take into account nonlinear terms in Eqs. (1.3). The simplest nonlinear effect can be shown using the quasi-neutral approximation ($n_i = n_e$) in the equations with no equilibrium flow. This approximation is valid for scales much larger than the Debye length (d_e). In this case the Eqs. (1.3) will have the form

$$\left(\frac{\partial}{\partial t} + \mathbf{v}_i \cdot \nabla\right) \ln(n_i) + \nabla \cdot \mathbf{v}_i = 0, \tag{1.10a}$$

$$\left(\frac{\partial}{\partial t} + \mathbf{v}_i \cdot \nabla\right) \mathbf{v}_i + c_s^2 \nabla \ln(n_i) = 0. \tag{1.10b}$$

It can be shown [20] that this system will lead us to

$$v_t + v v_z = 0 \tag{1.11}$$

Burgers-type equation. This equation has a general solution [21] in the form

$$v(z,t) = f(z - vt), \tag{1.12}$$

with the initial condition

$$v(z, t = 0) = f(z). \tag{1.13}$$

This solution was discovered by Riemann in 1860. The correctness of solution (1.12) can be verified by straightforward calculations. Using solution (1.12) one can obtain

$$v_z = \frac{f'}{1 + f't}, \tag{1.14a}$$

$$v_t = -\frac{v f'}{1 + f't}, \tag{1.14b}$$

where $f' = \frac{df}{d\xi}$, $\xi = z - vt$.

By substituting Eqs. (1.14) into Eq. (1.11) we can confirm that expression (1.12) is a solution. Let us consider the Gaussian initial condition (red solid line in Fig. 1.1). It follows from the solution that each point is moving with the velocity proportional to its amplitude, so the top of the bell is moving faster than other regions. The evolution of the Gaussian initial condition is illustrated in Fig. 1.1. We can see that the solution will tend to form a vertical front. The front of the solution steepens with time (dash-dotted green line in Fig. 1.1) until the gradient of the velocity becomes infinite ($v_z = \infty$). This happens when the denominators in Eqs. (1.14) are zeros. After that point in time, the profile of the velocity becomes a two-valued function (blue and yellow line on Fig. 1.1). This phenomenon is called wave breaking. Generally speaking, the equation (1.11) becomes invalid after this point.

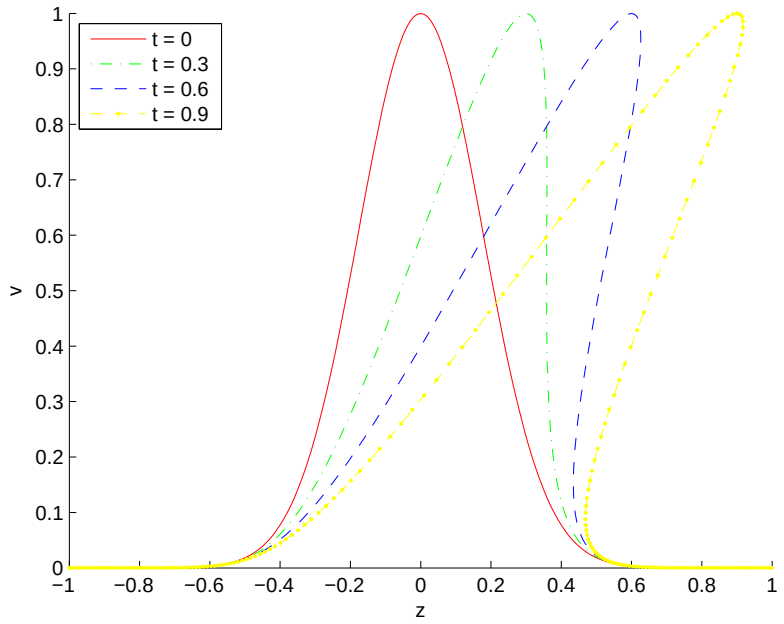

Figure 1.1: Example of wave breaking, the solution to the Burgers' equation (1.11).

1.1.3 Solitons

Nonlinear evolution of Eq. (1.11) leads to a multivalued solution. However, there are processes which may limit the wave breaking. For example, it could be the viscosity. In our case, the wave breaking is balanced by dispersion. Because of the dispersion, different

harmonics will travel with different velocities. This effect could balance the nonlinear wave breaking. For certain solution, when dispersion spreading is compensated by nonlinear steepening the stationary traveling solutions with finite amplitude called solitons may exist. To take dispersion into account one should include charge separation via Poisson equation (non quasi-neutrality). This dynamics could be described by Eqs. (1.3). For one-dimensional case

$$\frac{\partial n_i}{\partial t} + \frac{\partial (n_i v_i)}{\partial z} = 0, \tag{1.15a}$$

$$\frac{\partial v_i}{\partial t} + v_i \frac{\partial v_i}{\partial z} + \frac{e}{m_i}\frac{\partial \phi}{\partial z} = 0, \tag{1.15b}$$

$$\frac{\partial^2 \phi}{\partial z^2} = -4\pi e \left(n_i - n_0 \exp\left(\frac{e\phi}{T_e}\right)\right). \tag{1.15c}$$

To find the stationary solution to the equations (1.15), one can look for the waves traveling with the constant velocity U. This means that every function should depend on the variable $\xi = z - Ut$. This gives us

$$(n_i(v_i - U))' = 0, \tag{1.16a}$$

$$(\frac{v_i^2}{2} - U v_i' + \frac{e}{m_i}\phi)' = 0, \tag{1.16b}$$

$$\phi'' = -4\pi e \left(n_i - n_0 \exp\left(\frac{e\phi}{T_e}\right)\right), \tag{1.16c}$$

where the derivative is taken with respect to ξ.

Integrating the two first equations in (1.16) and assuming that in the equilibrium $v_i = 0$, $\phi = 0$, $n = n_0$, one obtains

$$\frac{\partial^2 \phi}{\partial \xi^2} = 4\pi e n_0 \left(\exp\left(\frac{e\phi}{T_e}\right) - \frac{1}{\sqrt{1 - 2\dfrac{e\phi}{m_i U^2}}}\right). \tag{1.17}$$

It is interesting to note that this equation could be rewritten in the form of nonlinear oscillator equation

$$\frac{\partial^2 \phi}{\partial \xi^2} = -\frac{dW(\phi)}{d\phi}, \tag{1.18}$$

where the artificial potential W is

$$W = -\sqrt{1-2\phi} - T\exp\phi/T + T + 1, \tag{1.19}$$

in dimensionless units ($\frac{e\phi}{m_i U^2} \to \phi, \frac{T_e}{m_i U^2} \to T, \frac{\xi\omega_{pi}}{U} \to \xi$). The integration constant was chosen so that $W(0) = 0$. From Eq. (1.19) it follows that $\phi < 1/2$. The violation of this condition results in wave breaking. Physically this means that for large amplitudes dispersion effects cannot stop wave breaking.

The artificial potential W can have two extrema: $\phi = 0$ and $\phi = \phi^*$. Depending on the value of T, the value of ϕ^* could be either positive or negative. When $T > 1$ the extremum is negative ($\phi^* < 0$). However, in this case the solution will not satisfy boundary conditions at infinity ($\phi \to 0$, when $\xi \to \pm\infty$). When $T < 1$ the nonzero extremum is positive, the axillary potential is shown on Fig. 1.2. The condition to avoid the wave breaking ($\phi < 1/2$) in dimensional units takes the form

$$U > c_s, \tag{1.20}$$

which means that solitons will travel faster than linear waves.

However, for solitons to exist we need one more condition which will exclude wave breaking

$$W(\phi = 1/2) > 0. \tag{1.21}$$

Finally Eqs. (1.20) and (1.21) will give us

$$c_s < U < U_c \sim 1.6 c_s. \tag{1.22}$$

Therefore, localized traveling solutions (solitons) will exist for velocities satisfying (1.22).

1.1.4 Sheath solution

In addition to the soliton solutions, equation (1.17) has very important stationary solutions which describe the plasma sheath.

We consider stationary solutions, so the time derivatives can be dropped. Then, one can

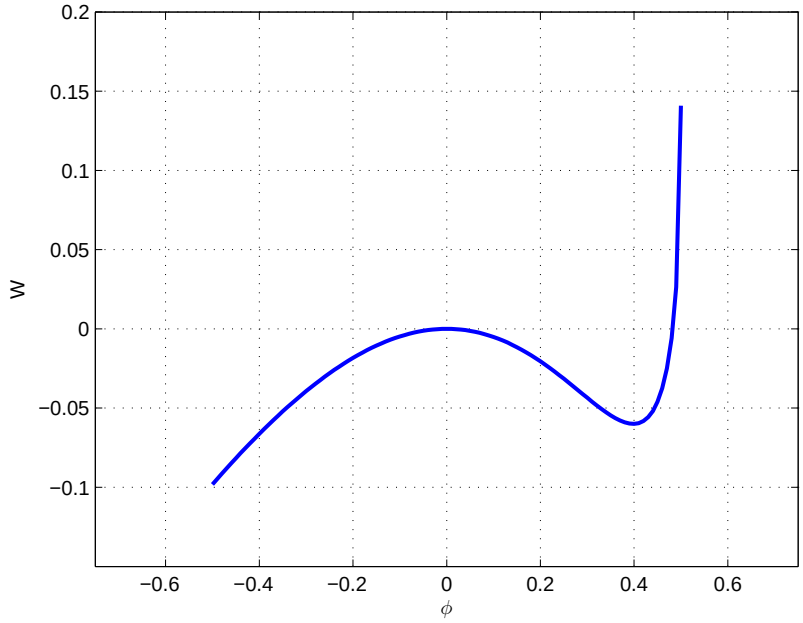

Figure 1.2: The axillary potential for nonlinear-oscillator equation (1.18) for $T_e < m_i U^2$ (also known as the Sagdeev potential).

write Eqs. (1.15) as (the first two equations were integrated)

$$n_i(z)v_i(z) = const, \tag{1.23a}$$

$$\frac{m_i v_i^2(z)}{2} + e\phi(z) = const, \tag{1.23b}$$

$$\frac{\partial^2 \phi}{\partial z^2} = -4\pi e \left(n_i - n_0 \exp\left(\frac{e\phi}{T_e}\right)\right). \tag{1.23c}$$

Where we assumed that ions have initial velocity U_s at $z = 0$. We cannot assume that ions are immobile at this point because in this case the system (1.23) will have no solution, so we assume that there is some pre-sheath region [22] where the weak electric field accelerates ions, until the system (1.23) gets a solution. We will show below that there is a condition on the speed of ions and we choose electrostatic potential to be zero at this point. Then the system (1.23) can be reduced to Eq. (1.17) where $U = U_s$. Integrating Eq. (1.17) and taking into account the boundary conditions $\phi(z = 0) = \phi'(z = 0) = 0$ (which means that at this

point the electric field is zero) we can write

$$\phi'^2 = 8\pi n_0 \left[T_e \left(\exp\left(\frac{e\phi}{T_e}\right) - 1 \right) + \frac{m_i U_s^2}{2} \left(\sqrt{1 - \frac{2e\phi}{m_i U_s^2}} - 1 \right) \right]. \tag{1.24}$$

The right side of this equation should be positive which means that the ion density must always be greater than the electron density in the sheath region, i.e. the sheath is electron deficient: the electrons leave the sheath region into the wall due to much higher mobility. There is some contradiction in choosing the electric field to be zero at $z = 0$ and postulating that the ion velocity is finite. This problem occurs due to a singular nature of the system at $z = 0$.

Expanding the right-hand side, one finds that for the existence of the sheath solution, $\phi'^2 > 0$, the following condition must be satisfied

$$U_s \geq c_s, \tag{1.25}$$

which is also known as the Bohm sheath condition.

Chapter 2

Analytical theory of waves and instabilities in plasmas with flows

In this section analytical theory for ion sound waves in a finite length system with ion flow is developed. The ions are assumed to be cold, so their dynamics is described by the equation of motion with zero pressure and continuity equations. The electrons are in thermodynamical equilibrium so their perturbed density follows a Boltzmann distribution. These are the conditions for ion sound waves described by equation (1.9). Normally, in an infinite (periodic) system, the addition of the equilibrium ion flow results in a Doppler shift of the basic (ion sound) mode. It is shown below that the addition of the walls with specific boundary conditions leads to the instability. The boundary conditions are those of the standard Pierce problem: these are natural physical boundary conditions for the case of the ion beam emitted from the left wall.

2.1 Infinite (periodic) systems

The system with an equilibrium ion flow $\mathbf{v}_0$ is described by equations similar to Eqs. (1.6) with the addition of the $\mathbf{v}_0 \cdot \nabla$ term to the convective derivative

$$\left(\frac{\partial}{\partial t} + \mathbf{v}_0 \cdot \nabla\right) n_i + n_0 \nabla \cdot \mathbf{v}_i = 0, \tag{2.1a}$$

$$\left(\frac{\partial}{\partial t} + \mathbf{v}_0 \cdot \nabla\right) \mathbf{v}_i + \frac{e}{m_i} \nabla \phi = 0, \tag{2.1b}$$

$$n_e = \frac{n_0 e}{T_e} \phi, \tag{2.1c}$$

$$\nabla^2 \phi = -4\pi e \left(n_i - n_e\right). \tag{2.1d}$$

At first, we consider the infinite system so the solution can be sought in the form of plane wave ($\sim e^{i(\mathbf{k}\cdot\mathbf{r}-\omega t)}$). In quasi-neutral approximation ($n_i = n_e$) one has

$$\omega = \mathbf{v}_0 \cdot \mathbf{k} \pm c_s k. \tag{2.2}$$

In general case, the dispersion equation takes the form

$$\omega = \mathbf{v}_0 \cdot \mathbf{k} \pm \frac{c_s k}{\sqrt{1 + k^2 d_e^2}}. \tag{2.3}$$

In infinite system, the role of the equilibrium flow is reduced to a simple Doppler shift in the frequency.

2.2 Finite length systems

In real systems we have boundaries which could affect wave dynamics in plasmas. To simplify this problem, we restrict ourselves to one-dimensional problem with two boundaries. To take those boundaries into account, we cannot look for a solution in $X \sim e^{i(\mathbf{k}\cdot\mathbf{r}-\omega t)}$ form, but replace it with a weaker form $X \sim e^{-i\omega t}$. Substituting this into Eqs. (2.1) and neglecting all dimensions except z

$$-i\omega n_i + v_0 \frac{\partial n_i}{\partial z} + n_0 \frac{\partial v_i}{\partial z} = 0, \tag{2.4a}$$

$$-i\omega v_i + v_0 \frac{\partial v_i}{\partial z} + \frac{e}{m_i} \frac{\partial \phi}{\partial z} = 0, \tag{2.4b}$$

$$n_e = \frac{n_0 e}{T_e} \phi, \tag{2.4c}$$

$$\frac{\partial^2 \phi}{\partial z^2} = -4\pi e \left(n_i - n_e\right). \tag{2.4d}$$

The boundary conditions are

$$\phi(z=0) = \phi(z=L) = n_i(z=0) = v_i(z=0) = 0, \tag{2.5}$$

where L is the length of the system.

In the general case this system can be reduced to the equation

$$v_0^2\phi'''' - 2i\omega v_0\phi''' + \left[\omega_{pi}^2 - \omega^2 - \frac{v_0^2}{d_e^2}\right]\phi'' + \frac{2i\omega v_0}{d_e^2}\phi' + \frac{\omega^2}{d_e^2}\phi = 0, \tag{2.6}$$

which clearly shows the singular nature of the perturbation due to a finite v_0. Obviously in the limit of $v_0 \to 0$ one obtains the dispersion equation in form of Eq. (1.9). Seeking solution to Eq. (2.6) in the form $\phi \sim e^{\lambda z}$ leads to the equation for λ

$$v_0^2\lambda^4 - 2i\omega v_0\lambda^3 + \lambda^2\left[\omega_{pi}^2 - \omega^2 - \frac{v_0^2}{d_e^2}\right] + \frac{2i\omega v_0}{d_e^2}\lambda + \frac{\omega^2}{d_e^2} = 0,$$

or, in more convenient form,

$$d_e^2\left(\lambda - \frac{i\omega}{v_0}\right)^2\left(\lambda^2 - \frac{1}{d_e^2}\right) + \frac{c_s^2}{v_0^2}\lambda^2 = 0, \tag{2.7}$$

which corresponds to Eq. (2.3).

2.2.1 Full quasi-neutrality case

Dispersion plays an important role in the instability mechanism. For length scales much longer than the Debye length, charge separation is not important and one can consider the fully quasi-neutral case, $n_i = n_e$, corresponding to the absence of the dispersion. In this limit, the system (2.4) will reduce to the form

$$\phi'' + \frac{2i\omega v_0}{c_s^2 - v_0^2}\phi' + \frac{\omega^2}{c_s^2 - v_0^2}\phi = 0, \tag{2.8}$$

where the prime is a derivative with respect to z.

The general solution of this equation has the form

$$\phi(z) = C_1 \exp\left(\frac{i\omega z}{v_0 + c_s}\right) + C_2 \exp\left(\frac{i\omega z}{v_0 - c_s}\right). \tag{2.9}$$

By imposing the condition (2.5), we obtain the equation for ω, which define C_1, C_2 and ω

$$\omega_n = \pi n \frac{v_0^2 - c_s^2}{L c_s}, n \in \mathbb{Z}. \tag{2.10}$$

It is worth to note that the Eq. (2.10) is not valid in the zero electron temperature limit, ($T_e \to 0$, $c_s \to 0$) because in this case the solution for the electrostatic potential will be different from Eq. (2.9)

$$\phi(z) = (C_1 + C_2 z) e^{\frac{i\omega}{v_0} z}, \tag{2.11}$$

while boundary conditions will give us the frequency

$$\omega_n = \frac{2\pi n}{L} v_0, n \in \mathbb{Z}. \tag{2.12}$$

Therefore, the non-dispersive waves are stable. As it will be shown below, the wave dispersion is crucial for the instability mechanism.

2.2.2 Weak dispersion case

In the long systems, $d_e \ll L$, the dispersion is weak, $kd_e \ll 1$, where the wave number $k \sim 1/L$. Using dispersion equation for plasma without flows (1.9), one gets the estimates for the mode frequency

$$\omega \sim k c_s \text{ or } \omega \sim \frac{d_e}{L} \omega_{pi}. \tag{2.13}$$

We solve Eq. (2.7) treating the Debye length as a small parameter; thus, it has four roots [23] where two of them are small $\sim O(1)$ and two of them are large $\sim O(1/d_e)$. The first pair coincides with those in the quasi-neutral case

$$\lambda_{1,2} = \frac{i\omega}{v_0 \pm c_s} + O(d_e^2) \sim O(1). \tag{2.14}$$

The second pair is

$$\lambda_{3,4} = \pm \frac{i}{v_0 d_e} \sqrt{c_s^2 - v_0^2} + \frac{i\omega c_s^2}{v_0} \frac{1}{c_s^2 - v_0^2} + O(d_e) \sim O(\frac{1}{d_e}). \tag{2.15}$$

Since all roots are different, we can write the general solution of Eq. (2.6) in the following form

$$\phi(z) = C_1 e^{\lambda_1 z} + C_2 e^{\lambda_2 z} + C_3 e^{\lambda_3 z} + C_4 e^{\lambda_4 z}. \tag{2.16}$$

The perturbed ion velocity and density from the full system (1.1) are found as

$$4\pi e n_i = \frac{\phi}{d_e^2} - \phi'', \tag{2.17}$$

$$4\pi e n_0 v_i = \frac{v_0}{d_e^2}\phi + \frac{c_s^2 - v_0^2}{i\omega d_e^2}\phi' - v_0\phi'' + \frac{v_0^2}{i\omega}\phi'''. \tag{2.18}$$

The dispersion equation is obtained as a condition for the existence of a nontrivial solution for C_1,C_2,C_3,C_4 in the linear system of equations (2.5)

$$D = det \begin{pmatrix} 1 & 1 & 1 & 1 \\ e^{\lambda_1 L} & e^{\lambda_2 L} & e^{\lambda_3 L} & e^{\lambda_4 L} \\ \lambda_1^2 & \lambda_2^2 & \lambda_3^2 & \lambda_4^2 \\ \mu_1 & \mu_2 & \mu_3 & \mu_4 \end{pmatrix} = 0, \tag{2.19}$$

where

$$\mu_k = \left(\frac{c_s^2}{v_0^2} - 1\right)\lambda_k + d_e^2\lambda_k^3. \tag{2.20}$$

The dispersion equation (2.19) is difficult to solve analytically as there are numerous solutions on the whole complex plane. However, we are interested only in those with the largest imaginary part, since these unstable modes will dominate. The numerical solution of Eq. (2.19) for the long system, with the length larger than the Debye length, $L = 10d_e$, is shown in Fig. 2.1a. The mode frequency is consistent with estimation (2.13).

For a fixed system length L, the instability growth rate depends on the dimensionless ion flow velocity v_0/c_s. The unstable regions are alternating with oscillatory ($\Re(\omega) \neq 0$) and aperiodic ($\Re(\omega) = 0$) zones. The boundaries of the zones could be found analytically using the fact that at the boundary the wave frequency is zero. Expanding Eq. (2.19) in a Taylor series

$$D(\omega) = D(0) + \frac{\partial D(0)}{\partial \omega}\omega + O(\omega^2) = 0, \tag{2.21}$$

and using that $D(0) \equiv 0$ and $\frac{\partial D(0)}{\partial \omega} = 0$, one finds

$$\frac{v_0^2}{c_s^2} = \frac{1}{1 + \pi^2 n^2 \frac{d_e^2}{L^2}} \text{ , where } n = 1, 2, 3.... \tag{2.22}$$

Solutions to equation (2.22) correspond to zones boundaries in Fig. 2.1.

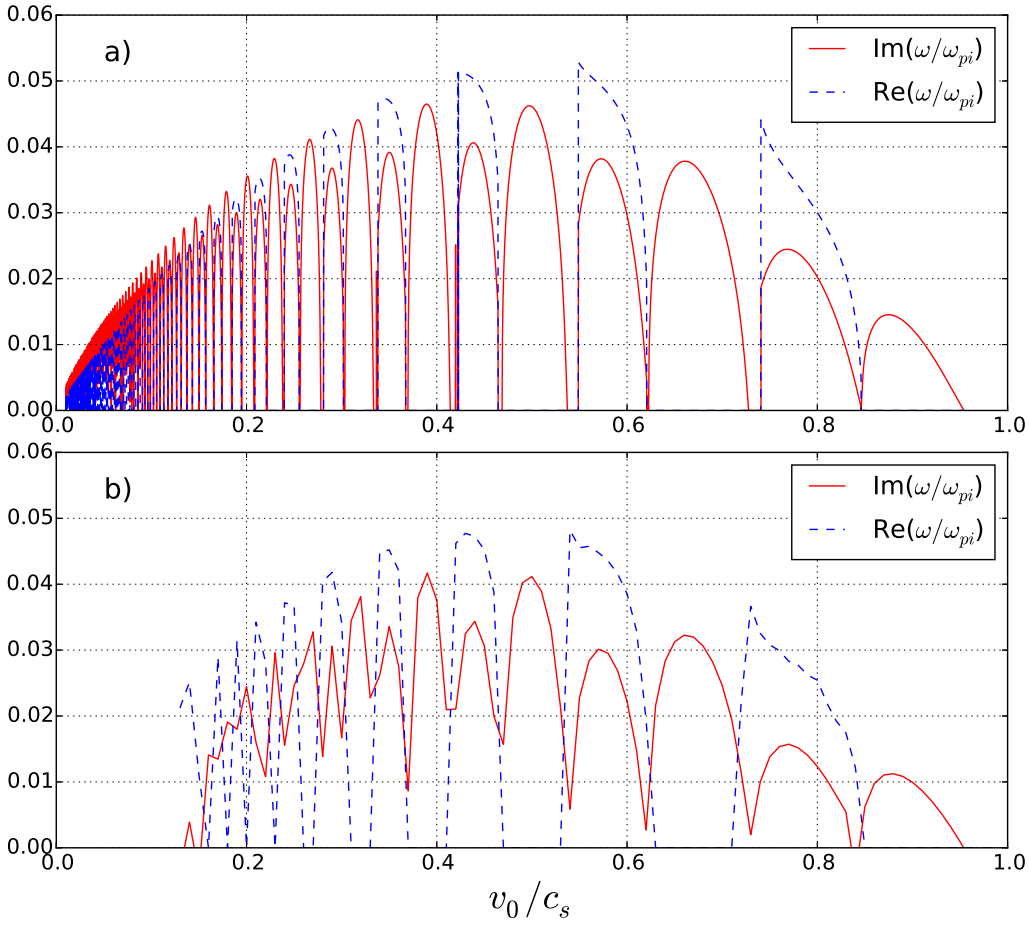

Figure 2.1: The alternating zones of aperiodic ($\Re(\omega) = 0$) and oscillatory ($\Re(\omega) \neq 0$) instabilities; a) the solution of the analytical dispersion equation (2.19), b) results of numerical simulations.

2.2.3 Strong dispersion case

In the short wavelength limit ($kd_e \gg 1$ or $d_e \gg L$), the dispersion modifies the solution. In this limit, the ion sound modes are reduced to the oscillations with the frequency of the order of $\omega \sim \omega_{pi}$. In this case, the reciprocal of the Debye length ($1/d_e$) is considered as a

small parameter. Then the roots of the Eq. (2.7) are [23]

$$\lambda_{1,2} = 0 \text{ and } \lambda_{3,4} = i\frac{\omega \pm \omega_{pi}}{v_0}, \tag{2.23}$$

and the general solution

$$\phi(z) = C_1 \exp\left(i\frac{\omega + \omega_{pi}}{v_0}z\right) + C_2 \exp\left(i\frac{\omega - \omega_{pi}}{v_0}z\right) + C_3 z + C_4. \tag{2.24}$$

This situation becomes mathematically equivalent to the Pierce instability. Imposing boundary conditions (2.5), one obtains an homogeneous linear system, which has nontrivial solutions when the following dispersion equation is satisfied

$$2\xi\alpha(1 - e^{i\xi}cos\alpha) + i(\xi^2 + \alpha^2)sin\alpha e^{i\xi} + i\frac{\xi^2}{\alpha}(\xi^2 - \alpha^2) = 0, \tag{2.25}$$

where $\xi = L\omega/v_0$ and $\alpha = L\omega_p/v_0$.

It was shown [13, 19] that the dispersion equation (2.25) has the following stability properties:

$$\alpha < \pi \qquad \text{- has stable solution,} \tag{2.26}$$

$$(2N-1)\pi < \alpha < 2N\pi \qquad \text{- has aperiodic instability,} \tag{2.27}$$

$$2N\pi < \alpha < (2N-1)\pi \qquad \text{- has oscillatory instability,} \tag{2.28}$$

where $N = 1, 2, 3....$, with a maximum growth rate $\gamma \sim v_0/L$.

There are many roots of the dispersion equation (2.25) on whole complex plane; as before, we choose only roots which have the largest imaginary part. The solutions which meet these criteria are shown in Fig. 2.2. The alternating aperiodic and oscillatory instability zones exist similar to the weak dispersion case. Fig. 2.1 also shows the results of direct initial value simulations described in the next section.

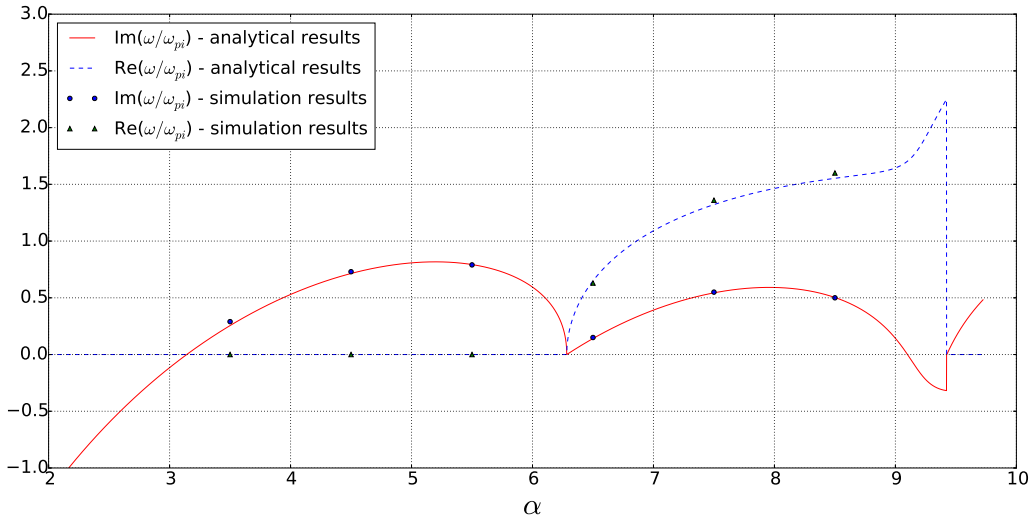

Figure 2.2: The oscillatory ($\Re(\omega) \neq 0$) and aperiodic ($\Re(\omega) = 0$) instabilities in strong dispersion case. The analytical solution of (2.25) and numerical simulations for $L = 0.1d_e$.

2.2.4 Traveling wave solution

We can try to solve Eqs. (2.1) in a different way. Let us rewrite it in the form

$$\omega_{pi}^2 \nabla^2 \phi = \left(\frac{\partial}{\partial t} + \mathbf{v}_0 \cdot \nabla \right)^2 \left(\frac{\phi}{d_e^2} - \nabla^2 \phi \right) \tag{2.29}$$

or in one-dimensional case

$$\omega_{pi}^2 \frac{\partial^2 \phi}{\partial z^2} = \left(\frac{\partial}{\partial t} + v_0 \frac{\partial}{\partial z} \right)^2 \left(\frac{\phi}{d_e^2} - \frac{\partial^2 \phi}{\partial z^2} \right). \tag{2.30}$$

Let us choose new variables as

$$\eta = z - v_0 t, \tag{2.31a}$$

$$\tau = t. \tag{2.31b}$$

Then

$$\frac{\partial}{\partial t} = -v_0 \frac{\partial}{\partial \eta} + \frac{\partial}{\partial \tau}, \tag{2.32a}$$

$$\frac{\partial}{\partial z} = \frac{\partial}{\partial \eta}, \tag{2.32b}$$

$$\frac{\partial}{\partial t} + v_0 \frac{\partial}{\partial z} = \frac{\partial}{\partial \tau}. \tag{2.32c}$$

Substituting this into Eq. (2.30), one has

$$\omega_p^2 \frac{\partial^2 \phi}{\partial \eta^2} = \left(\frac{\partial}{\partial \tau} \right)^2 \left(\frac{\phi}{d_e^2} - \frac{\partial^2 \phi}{\partial \eta^2} \right), \tag{2.33}$$

or,

$$\frac{\partial^2 \phi}{\partial \tau^2} - c_s^2 \frac{\partial^2 \phi}{\partial \eta^2} = d_e^2 \frac{\partial^4 \phi}{\partial \tau^2 \partial \eta^2}. \tag{2.34}$$

This is a homogeneous equation, so we can try separation of variables

$$\phi = T(\tau) R(\eta), \tag{2.35}$$

which leads us to the following equation

$$\frac{R}{R''} = d_e^2 + c_s^2 \frac{T}{T''}. \tag{2.36}$$

Since we cannot have an exponentially growing solution in space, for some κ we have

$$\frac{R}{R''} = -\frac{1}{\kappa^2} \tag{2.37}$$

which gives

$$R'' + \kappa^2 R = 0 \text{ and } T'' + \Omega^2 T = 0, \tag{2.38}$$

where Ω agrees with Eq. (1.9).

The approach described in this section is very appealing for infinite plasmas. However, in case of finite length systems with fixed boundaries all complexity described earlier are hidden in boundaries. After change of variables all boundary conditions will depend on time

producing the same level of complexity as before. The approach where problem is solved in the moving reference frame is often useful as has been discussed in literature [7, 24].

2.3 Excitation of low hybrid waves by the ion beam propagating perpendicular to the external field

It turns out the that mathematical structure of the equations we have studied so far is similar to a different problem which has important applications in electric propulsion and plasma processing, namely, to the problem of the excitation of low hybrid waves in Hall thrusters and magnetrons. Both of these devices have an external magnetic field so that the electrons are magnetized, $\rho_e \ll L$, which allows the trapping of electrons in the magnetic field. The magnetic field is weak so the ions are not magnetized due to their large Larmor radius, $\rho_i \gg L$. A typical Hall thruster configuration has cylindrical geometry with the electric field directed along the cylinder axis, while the magnetic field is mostly in radial direction. The schematic configuration of the Hall thruster is shown in Fig. 2.3, and the fields geometry in Fig. 2.4.

This type of electric propulsion has been widely and successfully used on various satellites due to its high efficiency and relatively simple construction [25]. However, despite successful applications, the nature of the electron transport in these devices is not fully understood [26], [27]. It is presumed that plasma fluctuations are the reason for enhanced transport. It was suggested that low hybrid modes may be excited due to finite length effects [12].

To describe simplest equilibrium state we will use two-fluid MHD equations with magnetized electrons and non-magnetized ions. Since we are trying to study the boundary effects, we are neglecting temperature effects ($T_e = T_i = 0$), all friction forces among different species and considering only a quasi-neutral case. For ion equilibrium we can write flow conservation (integrated continuity equation) $n_{i0}V_{i0} =$ constant and energy conservation (integrated Euler equation) $\frac{m_i V_{i0}^2(z)}{2} + e\phi_o(z) =$ constant, where V_{i0} is the projection on the z-axis, since it is the axis along the constant electric field. So we can see that in Hall truster, ions travel along cylinder axis with velocity $V_{i0} = \sqrt{V_{i00}^2 + \frac{2eE_0 z}{m_i}}$ where we have chosen $\phi(z = 0) = 0$ and $V_i(z = 0) = V_{i00}$ and assumed that the electric field is constant. As for electrons, in

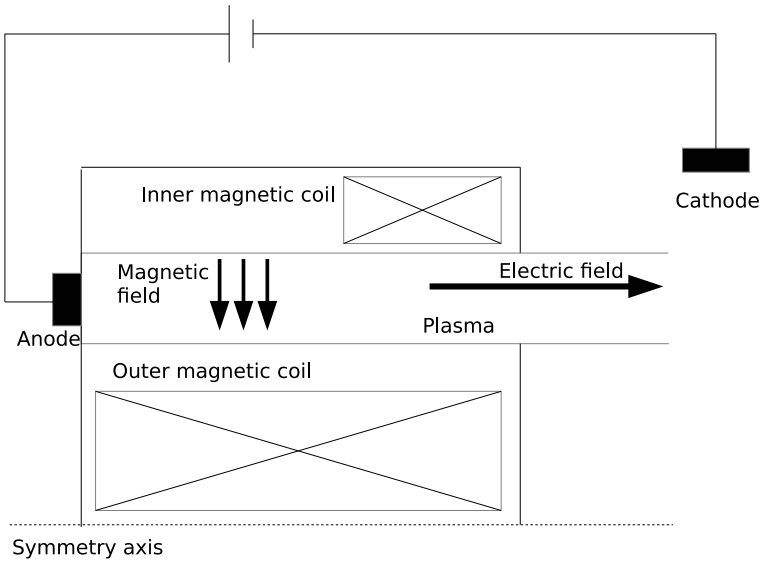

Figure 2.3: Schematic of the Hall thruster.

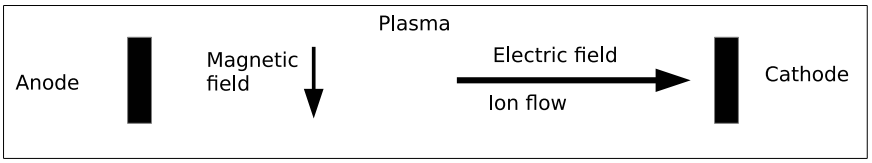

Figure 2.4: Geometry of the electric and magnetic field and flow.

the guiding center approximation they will rotate with "E×B" speed ($\mathbf{V_{e0}} = c\frac{E_0}{B_0}\hat{\mathbf{e}}_\phi$ where E_0 , B_0 - stationary electric and magnetic fields, $\hat{\mathbf{e}}_\phi$ - poloidal direction unit vector in Hall thruster cylinder.)

Let us consider quasi-neutral perturbation of ion and electron velocity with density as well as electrostatic potential dependent only on a z-direction. In this case linearized equations

will take the form

$$\frac{\partial V_{iz}}{\partial t} + V_{i0}\frac{\partial V_{iz}}{\partial z} + V_{iz}\frac{\partial V_{i0}}{\partial z} + \frac{e}{m_i}\frac{\partial \phi}{\partial z} = 0, \tag{2.39a}$$

$$\frac{\partial n}{\partial t} + n_0\frac{\partial V_{iz}}{\partial z} + V_{i0}\frac{\partial n}{\partial z} + V_{iz}\frac{\partial n_0}{\partial z} + n\frac{\partial V_{i0}}{\partial z} = 0, \tag{2.39b}$$

$$\frac{\partial V_{ex}}{\partial t} - \frac{e}{m_e}\frac{\partial \phi}{\partial z} + \frac{e}{m_e c}V_{ey}B_0 = 0, \tag{2.39c}$$

$$\frac{\partial V_{ey}}{\partial t} - \frac{e}{m_e c}V_{ex}B_0 = 0, \tag{2.39d}$$

$$\frac{\partial n}{\partial t} + n_0\frac{\partial V_{ex}}{\partial z} = 0, \tag{2.39e}$$

where V_{iz},V_{ex},V_{ey} - perturbation of ion and electron velocity, ϕ - perturbation of electrostatic potential, n - density perturbation.

The boundary conditions for perturbations are

$$\phi(0) = \phi(L) = n(0) = V_{iz}(0) = 0. \tag{2.40}$$

As previously, we assume time dependence in the form $X(z,t) = X(z)e^{-i\omega t}$ having

$$-i\omega V_{iz} + V_{i0}\frac{\partial V_{iz}}{\partial z} + V_{iz}\frac{\partial V_{i0}}{\partial z} + \frac{e}{m_i}\frac{\partial \phi}{\partial z} = 0, \tag{2.41a}$$

$$-i\omega n + n_0\frac{\partial V_{iz}}{\partial z} + V_{i0}\frac{\partial n}{\partial z} + V_{iz}\frac{\partial n_0}{\partial z} + n\frac{\partial V_{i0}}{\partial z} = 0, \tag{2.41b}$$

$$\frac{\partial^2 \phi}{\partial z^2} = \frac{n m_e}{n_0 e}(\omega^2 - \omega_{ce}^2), \tag{2.41c}$$

where $\omega_{ce} = \frac{eB_0}{m_e c}$ electron-cyclotron frequency. Assuming that the ion equilibrium velocity is constant in space ($V_{i0} \sim$ const) and the frequency of the considered perturbation is much smaller than electron cyclotron frequency ($|\omega| \ll |\omega_{ce}|$) we have

$$-i\omega n + V_{i0}\frac{\partial n}{\partial z} + n_0\frac{\partial V_{iz}}{\partial z} = 0, \tag{2.42a}$$

$$-i\omega V_{iz} + V_{i0}\frac{\partial V_{iz}}{\partial z} + \frac{e}{m_i}\frac{\partial \phi}{\partial z} = 0, \tag{2.42b}$$

$$\frac{\partial^2 \phi}{\partial z^2} = -\frac{m_e \omega_{ce}^2}{e n_0}n. \tag{2.42c}$$

These equations lead to equation mathematically equivalent to Pierce dispersion equations (Section 2.2.3). So dispersion equation will be the same as Eq. (2.25) if we replace $\alpha \rightarrow \alpha_h = \frac{\omega_{lh} L}{V_{i0}}$ where $\omega_{lh} = \sqrt{\omega_{ce}\omega_{ci}} = \frac{eB_0}{c\sqrt{m_i m_e}}$ and $\xi \rightarrow \xi_h = \frac{L\omega}{V_{i0}}$. From this it follows that in this situation we will have all instabilities discussed in section 2.2.3.

In the limit of zero ion velocity and no boundaries, transverse electrostatic oscillations are possible, referred to as so-called lower hybrid waves. Plugging $n, V_{iz}, \phi \sim e^{i(kz-\omega t)}$ into Eqs. (2.41) and neglecting flows, the dispersion equation will be

$$\omega^2 = \frac{\omega_{ce}^2}{1 + \frac{m_i}{m_e}} \approx \frac{m_e}{m_i}\omega_{ce}^2 \equiv \omega_{lh}^2, \tag{2.43}$$

where ω_{lh}^2 is a lower hybrid frequency.

Hall thrusters are very important propulsion devices which are widely used in space missions. Unfortunately, they are not fully understood yet. The main unsolved issue is anomalous transport which dramatically decreases efficiency. Plasma fluctuations are believed to be the main reason for this transport. Lower hybrid modes excited due to finite length effects could be an important sources of such plasma fluctuations.

Chapter 3

Numerical methods, algorithms and parallelization

Exact analytical solution of the systems discussed are not always possible, which requires a numerical solution. The nature of this system suggests that the solution will be a combination of traveling waves, which imposes some constraints on the choice of numerical methods. Moreover our system consists of two different types of equations that require different numerical algorithms. Different methods have been investigated and we have chosen those which are easier to generalize for nonlinear case and simple to parallelize. Here we consider a linearized version of the discussed problem.

3.1 Dimensionless equations

For numerical studies, it is often convenient to rewrite the equations into dimensionless form. Let us introduce

$$n^* = \frac{n}{n_0}, z^* = \frac{z}{d_e}, \phi^* = \frac{e\phi}{T_e}, t^* = t\omega_{pi}, v_0^* = \frac{v_0}{c_s}.$$

This scaling transforms the system (2.4) into the following equations (stars were omitted for convenience)

$$\frac{\partial n}{\partial t} + v_0 \frac{\partial n}{\partial z} + \frac{\partial v}{\partial z} = 0, \tag{3.1a}$$

$$\frac{\partial v}{\partial t} + v_0 \frac{\partial v}{\partial z} + \frac{\partial \phi}{\partial z} = 0, \tag{3.1b}$$

$$\frac{\partial^2 \phi}{\partial z^2} = \phi - n. \tag{3.1c}$$

It is important to note that the scale of the wave phase velocity is $v_\phi \sim \pm 1 + v_0$ ($\pm c_s + v_0$ in dimension form). Thus, in the long wave length limit, dimensionless value $v_0 = 1$ separates two situations: (a) $v_0 > 1$ - waves are traveling only in one direction; (b) $v_0 < 1$ - waves are traveling in both directions.

3.2 Numerical methods

The above system (3.1) cannot be solved in time explicitly because the Poisson equation (3.1c) is implicit in time. Thus we divide our initial value problem into two sub-problems:

1. The explicit initial value problem (IVP), which can be advanced in time

$$\frac{\partial n}{\partial t} + v_0 \frac{\partial n}{\partial z} + \frac{\partial v}{\partial z} = 0, \tag{3.2a}$$

$$\frac{\partial v}{\partial t} + v_0 \frac{\partial v}{\partial z} + \frac{\partial \phi}{\partial z} = 0, \tag{3.2b}$$

$$\phi(z), n(t = 0, z), v(t = 0, z). \text{ - given.} \tag{3.2c}$$

2. The Poisson equation which is a boundary value problem (BVP)

$$\frac{\partial^2 \phi}{\partial z^2} = \phi - n, \tag{3.3a}$$

$$\phi(0) = \phi(L) = 0, \tag{3.3b}$$

$$n(z) \text{ - given.} \tag{3.3c}$$

Systems (3.3) and (3.2) are solved in time with the following algorithm implemented iteratively on each time step. We set up the initial profiles of ion density and velocity. The Poisson equation (3.3a) is solved at the beginning of each time step. It uses given ion density profile (either from the initial condition or from previous time step) to produce the electrostatic potential profile. The known potential distribution allows us to solve Eqs. (3.2) in time. This gives us new ion density and velocity profiles. The above algorithm is illustrated in Fig. 3.1.

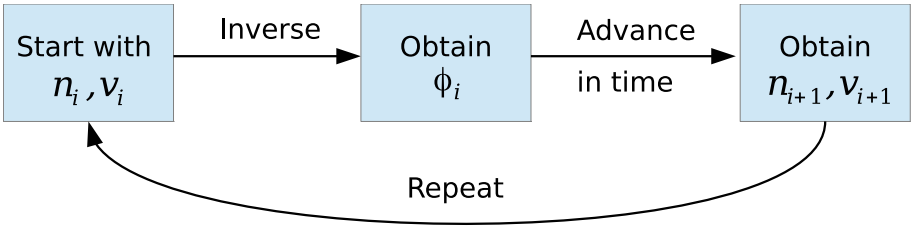

Figure 3.1: Algorithm for the solution of Eqs. (3.1).

3.2.1 Multiple shooting method

Commonly, the shooting methods [28] and finite difference schemes [29] are the methods of choice for a BVP. We implemented a shooting method due to its simplicity. We chose multiple shooting method (MSM) because it is easy to parallelize, has no disadvantages of simple shooting methods (e.g., limitations on a system length) [30], and (since our system is linear) MSM reduces to a system of IVPs and linear system of equations. To apply the multiple shooting method to the system (3.3), it is common to write it in the form

$$\frac{\partial \mathbf{y}}{\partial z} = A \cdot \mathbf{y} + \mathbf{b}, \tag{3.4a}$$

$$B_0 \cdot \mathbf{y}(0) + B_L \cdot \mathbf{y}(L) = 0, \tag{3.4b}$$

$$\mathbf{b}(z) \text{ - given}, \tag{3.4c}$$

where

$$\mathbf{y} = \begin{pmatrix} \phi \\ \dfrac{\partial \phi}{\partial z} \end{pmatrix}, \mathbf{b} = -\begin{pmatrix} 0 \\ n \end{pmatrix} A = \begin{pmatrix} 0 & 1 \\ 1 & 0 \end{pmatrix}, B_0 = \begin{pmatrix} 1 & 0 \\ 0 & 0 \end{pmatrix}, B_L = \begin{pmatrix} 0 & 0 \\ 1 & 0 \end{pmatrix}.$$

In the multiple shooting method we divide the domain into many small subintervals. On every subinterval, we have the IVP with artificial initial conditions as shown in Fig. 3.2.

The solution on every subinterval is given by

$$\mathbf{y_n}(z, \mathbf{c_{n-1}}) = Y_n(z)\mathbf{c_{n-1}} + \mathbf{v_n}(z), \text{ where } Y_n(z) = \begin{pmatrix} \cosh(z - z_{n-1}) & \sinh(z - z_{n-1}) \\ \sinh(z - z_{n-1}) & \cosh(z - z_{n-1}) \end{pmatrix}.$$

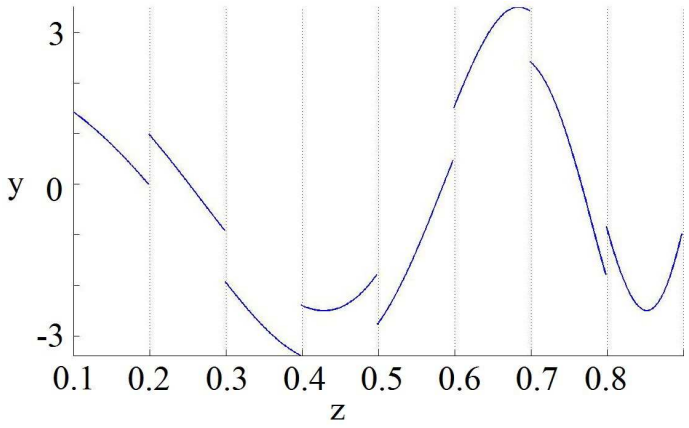

Figure 3.2: Set of IVPs on subintervals ($0 = z_0 < z_1 < ... < z_N = L$).

Y_n is the fundamental solution, $\mathbf{v_n}(z)$ is some particular solution with zero initial conditions, and $\mathbf{c_{n-1}}$ is the patching coefficients which is determined from boundary conditions on subintervals. The next key step of multiple shooting method is to impose equations that provide continuity of the solution and satisfy the boundary conditions. At this step, we obtain a number of algebraic equations to solve. In our case due to linearity of Eqs. (3.4) we have the following linear system

$$\mathbf{Ac} = \mathbf{r},$$

where

$$\mathbf{A} = \begin{pmatrix} -Y_1(z_1) & I & & & \\ & -Y_2(z_2) & I & & \\ & & ... & & \\ & & & -Y_{N-1}(z_{N-1}) & I \\ B_0 & & & & -B_L Y_N(L) \end{pmatrix},$$

$$\mathbf{c} = \begin{pmatrix} \mathbf{c_0} \\ \mathbf{c_1} \\ \dots \\ \mathbf{c_{N-2}} \\ \mathbf{c_{N-1}} \end{pmatrix}, \qquad \mathbf{r} = \begin{pmatrix} \mathbf{v_1}(z) \\ \mathbf{v_2}(z) \\ \dots \\ \mathbf{v_{N-1}}(z) \\ -B_L\mathbf{v_N}(L) \end{pmatrix}$$

Thus, the solution of the original BVP by MSM consists of two principal steps:

1. Solve IVPs on subintervals. In our case, we use fourth order Runge-Kutta method. Pseudo-code for serial implementation is shown below:

```
A = Fundamental solution;
Find B with IC at 0;
for i = sub interval do
|  B = RK4(IC=C(i));
end
G = GE(A,B);
for i = sub interval do
|  φ = RK4(IC = C(i));
end
```

2. Because Eqs. (3.4) are linear, our system of algebraic equations is linear, so we can use Gaussian elimination (GE) method [31] to obtain a solution. Illustration for the algorithm is given below:

```
for k = 1 ... m: do
|  Find pivot for column k;
|  i_max := argmax (i = k ... m, abs(A[i, k]));
|  if A[i_max, k] = 0 then
|  |  error "Matrix is singular!"
|  end
|  swap rows(k, i_max);
|  Do for all rows below pivot;
|  for  i = k + 1 ... m: do
|  |  Do for all remaining elements in current row;
|  |  for j = k ... n: do
|  |  |  A[i, j] := A[i, j] - A[k, j] * (A[i, k] / A[k, k])
|  |  end
|  |  Fill lower triangular matrix with zeros: A[i, k] := 0
|  end
end
```

3.2.2 Godunov scheme

The next step is to solve IVP (3.2) in time. It is a system of hyperbolic PDEs, which can be expressed in a conservative form. This fact is related to the nature of continuity and Euler equations, which are conservative

$$\frac{\partial \mathbf{U}}{\partial t} + \frac{\partial \mathbf{F}(\mathbf{U})}{\partial z} = 0, \tag{3.5}$$

where

$$\mathbf{U} = \begin{pmatrix} n \\ v \end{pmatrix}, \mathbf{F} = \begin{pmatrix} v_0 n + v \\ v_0 v + \phi \end{pmatrix}.$$

This form suggests to treat our system with a class of finite volume methods [32]. At the beginning we choose the simplest first-order upwind scheme [33], because for the high velocity of the ion flow we know that the waves propagate only in one direction. The simplest upwind scheme is given by

$$\mathbf{U}_j^{n+1} = \mathbf{U}_j^n + \frac{\Delta t}{\Delta z}(\mathbf{F}_j^n - \mathbf{F}_{j-1}^n).$$

However, we cannot use this scheme for the situations when the waves propagate in opposite directions. Let's define matrix $\hat{\mathbf{A}}$ as

$$\hat{\mathbf{A}} = \frac{\partial \bar{\mathbf{F}}}{\partial \bar{\mathbf{u}}}.$$

The eigenvalues of this matrix have physical interpretation. They are phase velocities of waves. So when λ_1, λ_2 eigenvalues of $\hat{\mathbf{A}}$ have different signs the waves propagate in opposite direction and we have to use more advanced methods. This is due to the fact that the upwind scheme calculates the next point in time ($U(t + \Delta t, z)$) based on two points located back in space and time ($U(t, z)$,$U(t, z - \Delta z)$), so when we have waves traveling in one direction, hyperbolic PDE exact domain of dependence are included on approximate domain of dependence. However, in our case there are waves propagating in both directions and approximate domain of dependence is no longer subset of exact domain. In other words, those waves will make the upwind scheme unconditionally unstable. To treat this issue we used

Lax-Friedrichs [32] and Harten, Lax, Van Leer (HLL) [34] methods. Lax-Friedrichs scheme shows quite nice results, and it is much simpler than HLL methods, but it requires high discretization for correct results due to high numerical viscosity. Another drawback is that when solution contains large gradients (sharp edges), it could exhibit the Gibbs phenomenon (type of numerical instability). The Lax-Friedrichs scheme is written in the form

$$u_i^{n+1} = \frac{1}{2}(u_{i+1}^n + u_{i-1}^n) - a\frac{\Delta t}{2\,\Delta x}(u_{i+1}^n - u_{i-1}^n).$$

We also tried MacCormack method, but it showed oscillatory behavior, since it has no numerical viscosity as Lax-Friedrichs method. In such situations the family of Godunov methods can be of interest. Such schemes use the solution of Riemann problem on computational cells. There are two classes of methods: approximate Riemann solvers and exact Riemann solvers. We used one kind of approximate Riemann solver - the HLL method, which assumes a Riemann solution consisting of just two waves separating three constant states. If ${s^R}_{i-1/2}$ and ${s^L}_{i-1/2}$ are upper and lower bounds of wave velocities respectively, the solution can be expressed as

$$\tilde{\mathbf{u}}(x,t) = \begin{cases} \mathbf{u_{i-1}} & \text{if } \dfrac{x}{t} \leq {s^L}_{i-1/2}, \\ {\mathbf{u^{HLL}}}_{i-1/2} & \text{if } {s^L}_{i-1/2} \leq \dfrac{x}{t} \leq {s^R}_{i-1/2}, \\ \mathbf{u_i} & \text{if } {s^R}_{i-1/2} \leq \dfrac{x}{t}. \end{cases}$$

Where intermediate state is obtained as

$${\mathbf{u^{HLL}}}_{i-1/2} = \frac{{s^R}_{i-1/2}\mathbf{u_i} - {s^L}_{i-1/2}\mathbf{u_{i-1}}}{{s^R}_{i-1/2} - {s^L}_{i-1/2}} - \frac{\mathbf{f_i} - \mathbf{f_{i-1}}}{{s^R}_{i-1/2} - {s^L}_{i-1/2}}.$$

The HLL flux can be found in the form

$$\mathbf{f_{i-1/2}} = \begin{cases} \mathbf{f_{i-1}} & \text{if } \dfrac{x}{t} \leq {s^L}_{i-1/2}, \\ \mathbf{f^{HLL}}_{i-1/2} & \text{if } {s^L}_{i-1/2} \leq \dfrac{x}{t} \leq {s^R}_{i-1/2}, \\ \mathbf{f_i} & \text{if } {s^R}_{i-1/2} \leq \dfrac{x}{t}. \end{cases}$$

And an intermediate flux is

$$\mathbf{f^{HLL}}_{i-1/2} = \frac{{s^R}_{i-1/2}\mathbf{f_{i-1}} - {s^L}_{i-1/2}\mathbf{f_i} + {s^R}_{i-1/2}{s^L}_{i-1/2}(\mathbf{u_i} - \mathbf{u_{i-1}})}{{s^R}_{i-1/2} - {s^L}_{i-1/2}}.$$

We can estimate upper and lower bounds of waves velocity from the expression for the phase velocity (2.3)

$$s^{R,L} = v_0 \pm \frac{1}{\sqrt{1 + k_{max}^2}}, \tag{3.6}$$

where $k_{max} = \frac{1}{L}$.

Thus, we use upwind scheme, when both waves propagate in one direction and HLL method when waves go in the opposite directions. The logic of the code for HLL scheme is introduced below

```
Calculate s_l and s_r as v_0 ± 1;
for k = 1 ... N: do
    Initialize local v and n;
    if s_l > 0 then
        Calculate flow with upwind scheme;
        update local v and n;
    end
    if s_r < 0 then
        Calculate flow with backward scheme;
        update local v and n;
    end
    if s_l ≤ 0 and s_r ≥ 0 then
        Calculate flow with HLL scheme;
        update local v and n;
    end
    Update global v and n;
end
```

As usual for finite difference methods for solving hyperbolic PDEs HLL method has the restrictions on Δt and Δx, which is called a Courant-Friedrichs-Lewy (CFL) condition and can be presented as [35]

$$C = \Delta t \sum_{i=1}^{n} \frac{u_{x_i}}{\Delta x_i} \leq C_{max}.$$

where u is the magnitude of the velocity, Δt is the time step Δx is the length interval. So, the space step Δx usually was chosen according to the time step Δt. For multiple shooting method the common measure of the error is the $\exp(L)$, where L is the length of sub-interval. Our goal is to choose number of intervals large enough to reduce the error, but no too large, because it will cause the increasing of Gaussian elimination operations, which are quite expensive in terms of the processor time. After a number of experiments it was discovered that for most cases we do not need more than 10 subintervals.

3.3 Code structure

In the pursuit of an object-oriented approach a class NIonBeam was created which serves as a storage for all methods and functions which we need to perform simulations. Class

Function	Description
NIonBeam(const char* IFN,int flag)	Constructor to create initial conditions
NIonBeam(const char* IFN,const char* OFN)	Main constructor to start simulation
GetIC()	Read initial contitions from file
WriteResultsTo(const char* filename)	Write results to files
RandomIC (double amplitude)	Generate random IC
GaussIC (double amplitude,double scale,double position)	Generate Gauss distributed IC
SinIC (double amplitude,double fr)	Generate sime distributed IC
UniformIC (double amplitude)	Generate uniform IC
NIonBeam()	Destructor

Table 3.1: List of accessory functions used in project

contains both versions of functions with and without parallelization. Moreover, we wanted to compare different numerical methods, or use their combinations, so there are several additional functions for different schemes. There are functions to create initial conditions and to read and write data to files. The full list of accessory functions is given in Table 3.1.

The full list of numerical methods and supplementary functions is given in Table 3.2.

The following functions were parallelized: MShooting(), HLL(), NIonBeam(const char* IFN,const char* OFN). All above mentioned functions can be called from the main program: main.c.

3.4 Parallel implementation

In order to be able to calculate large systems with high resolution parallelization of the code becomes necessary.

3.4.1 Parallelization of numerical methods using MPI.

A large popularity of distributed memory systems and their ability to work with enormous amount of data leads us to a Message Passing Interface (MPI) library, which is one of the most flexible and convenient tools to work with distributed memory systems [36]. Because, our problem consists of two separate tasks (BVP and IVP), it is best to parallelize those two

Function	Description
NIonBeam::Shooting ()	Single shooting method
MShooting(int number)	Multiple shooting method
LaxFriedrichs()	Lax-Friedrichs method
MacCormac()	Maccormac method
HLL()	HLL method
MShooting_Create_FM()	Create matrix with fundamental solution for IVPs
gauss_eliminate(double *a, double *b, double *x, int n)	Gaussian elimination
RK4_2d_shooting(double a)	Runge-Kutta to use in single shooting
RK4_MSH_V(int t1,int t2,double *v1,double *v2)	Runge-Kutta to use in multiple shooting to update v and n
RK4_MSH(double *s,int number)	Runge-Kutta to use in multiple shooting to update ϕ
swap_row(double *a, double *b, int r1, int r2, int n)	Swap row function for Gaussian Elimination

Table 3.2: List of numerical methods and supplementary functions used in project

problems separately.

1. **MPI parallelization for multiple shooting.** To solve the system of linear equations, it is common to use Gaussian elimination (GE) [37]. Initially, we planned to parallelize this part of the code as well however, as we mentioned above, number of subintervals when we wanted to execute GE is around 10. It means that the ratio of the number of spatial steps for the upwind scheme to the number of steps for multiple shooting is about $10^3 - 10^4$. It means, that the time which our code spends on these calculations is relatively small. Typically for our task, size of the matrix was about 32x32 and execution time of the serial version was about 10ms per iteration. As a result, we decided to leave this part of the code in the serial form for now. Algorithm for parallel multiple shooting implementation is shown below.

```
if rank == 0 then
|  A = Fundamental solution;
end
for i=local_start...local_end do
|  B = RK4(IC=(i));
end
for i = sub interval do
|  B = RK4(IC=C(i));
end
GATHER all data to process with rank = 0;
if rank == 0 then
|  G = GE(A,B);
end
SCATTER G to each process;
for i=local_start...local_end do
|  φ = RK4(IC = C(i));
end
```

2. **MPI parallelization for HLL scheme.** First, we should divide our space domain into equal pieces for each processor. It is important to note that those sub-domains should intersect (this intersection is called boundary buffer). Next, we should scatter the initial conditions on those sub-domains from the main processor. Solve all subintervals separately. The MPI parallelization algorithm is illustrated on Fig. 3.3. Below one can see the pseudo-code for HLL scheme:

```
Calculate s_l and s_r as v_0 ± 1;
if rank == 0 then
    Send first and last element of the subinterval to processor = rank - 1;
    Receive first and last element of the subinterval to processor = rank - 1;
end
if rank == P - 1 then
    Send first and last element of the subinterval to processor = rank + 1;
    Receive first and last element of the subinterval to processor = rank + 1;
end
for i=local_start...local_end do
    Initialize local v and n;
    if s_l > 0 then
        Calculate flow with upwind scheme;
        update local v and n;
    end
    if s_r < 0 then
        Calculate flow with backward scheme;
        update local v and n;
    end
    if s_l ≤ 0 and s_r ≥ 0 then
        Calculate flow with HLL scheme;
        update local v and n;
    end
    Update global v and n;
end
```

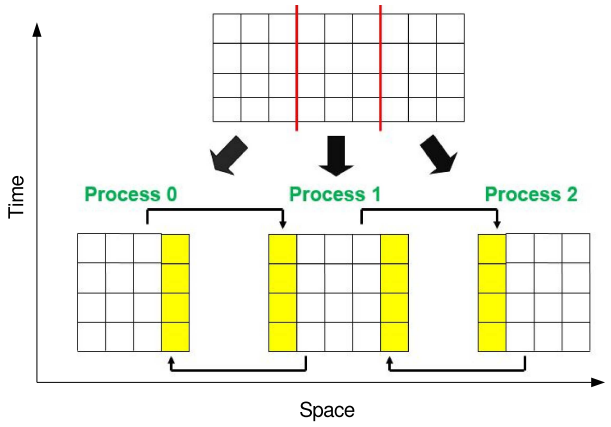

Figure 3.3: MPI parallelization for upwind scheme. Each processor solves in time separate space interval.

3.4.2 Parallelization of numerical methods using OpenMP.

In addition to distributed memory systems we decided to parallelize our code for shared memory systems with the OpenMP library.

OpenMP can be a good alternative to MPI when there is no access to distributed memory systems. Shared memory system can be a good choice for current personal workstations which become more powerful and can be considered as almost like shared-memory systems. The OpenMP has another advantage. The OpenMP library provide higher level of abstraction in parallel programming compared the MPI. Low-level parallel programming libraries (e.g. MPI) which allow you to control low level processes is more complicated. This complication usually decreases the efficiency of the programs. There is an opinion that "non-trivial multi-threaded programs are incomprehensible to humans" [38].

Parallelization algorithms using the OpenMP is close to that we choose for the MPI. However, there is a difference. When using the OpenMP library one should be careful with variable scope. It is impossible to enclose variables in shared clause in OpenMP when they are not declared. So class variables are not declared until the instance of class is not declared. Algorithm is presented below.

```
# pragma;
for i=1 ... N do
  | A = 0;
end
# pragma single;
for i=1 ... N do
  | A = Fundamental solution;
end
# pragma;
for i=1 ... N do
  | B = RK4(IC=C(i));
end
# pragma single;
for i=1 ... N do
  | φ = RK4(IC = C(i));
end
```

Parallelization of the Godunov method is done in a very simple way. We initialize n and

v values as local variables on master processor. Then we computed next values for n and v in parallel. Finally, we update global n and v on master processor. The algorithm is shown below.

```
# pragma single;
for i=1 ... N do
    initialize local_n and local_v ;
end
# pragma ;
for i=1 ... N do
    if s_l > 0 then
        Calculate flow with upwind scheme;
        update local_n and local_v;
    end
    if s_r < 0 then
        Calculate flow with backward scheme;
        update local_n and local_v;
    end
    if s_l ≤ 0 and s_r ≥ 0 then
        Calculate flow with HLL scheme;
        update local_n and local_v;
    end
end
# pragma single;
for i=1 ... N do
    Update global v and n;
end
```

3.5 Parallel scalability

Two versions of software (OpenMP and MPI) were tested on Westgrid cluster Nestor (*https://www.westgrid.ca/*). Two types of initial data sets were used with high and low time and space resolutions. This allows as to test speedup with different ratios of communication and calculation time. Execution time and speedup as a function of processors number are shown on Figs. 3.4, 3.5. The graph shows the efficiency of parallelization.

It is seen that OpenMP implementation speedup decreases when number of processors

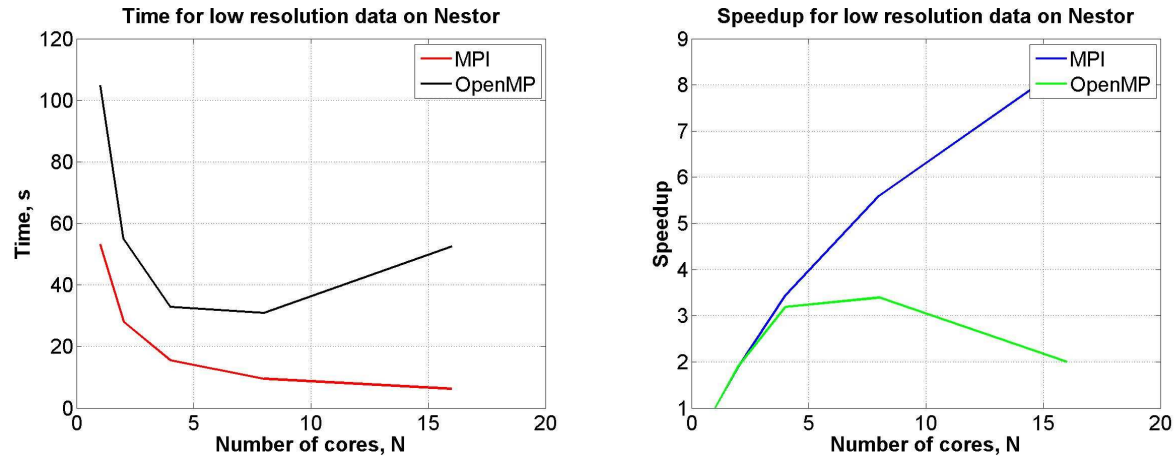

Figure 3.4: Execution time and speedup as a function of processors number for low resolution data with MPI and OpenMP on Nestor.

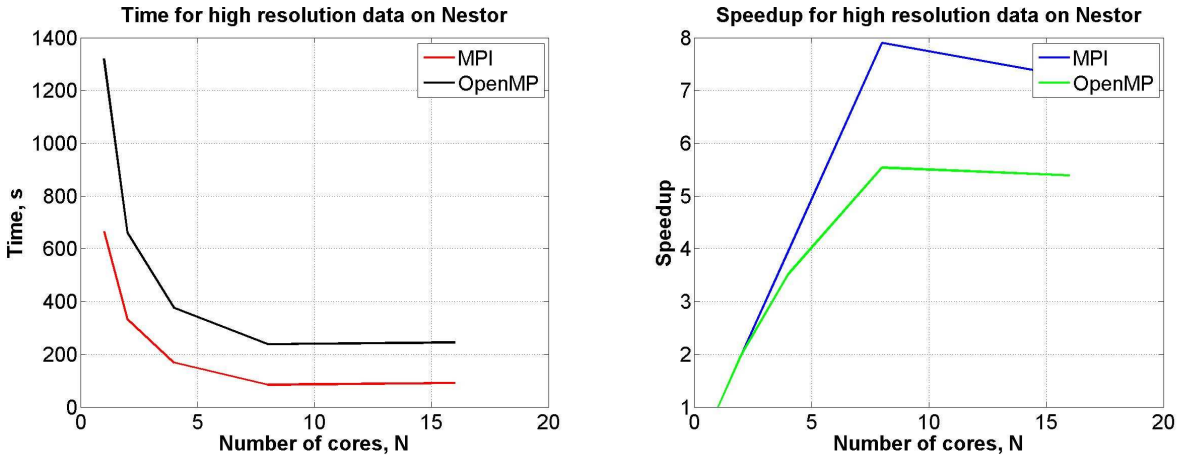

Figure 3.5: Execution time and speedup as a function of processors number for high resolution data with MPI and OpenMP on Nestor.

become higher than 8 which means that one node has only 8 cores.

MPI implementation also become slow when we using more than one node (more than 8 cores) which confirm the fact that interconnection between the nodes is much slower than between the cores.

Comparing data with high and low resolutions, we see that when communication over computation time ratio is decreasing the time scalability becomes much better.

Chapter 4

Simulation results

The purpose of this work is to study some general properties of plasma systems with the ion beam and develop numerical tools for the initial value problem of the eigen modes evolution. The final goal would be to investigate the nonlinear stage of the related instability. At this stage we have tested the linear module of the numerical code.

The results of numerical simulations are compared with analytical results for weak and strong dispersion cases. We start our simulations with initial conditions of a uniformly distributed random noise (e.g. Fig. 4.1) and observe the evolution of the following quantities

$$N^2 = \int_0^L n^2(z)dz,\ \Phi^2 = \int_0^L \phi^2(z)dz,\ V^2 = \int_0^L v^2(z)dz. \tag{4.1}$$

Depending on the value of input parameters (L, v_0) damped (stable) or growing (unstable) solutions were observed; examples of (4.1) evolution are shown on Figs. 4.2, 4.3, 4.4. Unstable solutions were fitted to the following curves

$$N^2, V^2, \Phi^2 \sim \cos(2\Re(\omega)t + \theta)e^{2\gamma t}, \tag{4.2}$$

to determine the real frequencies and growth rates.

When the length of the system exceeds the Debye length ($L \sim 10d_e$), the weak dispersion results are recovered. Example of frequency and growth rate dependence as a function of the ion flow velocity v_0 are shown in Figs. 2.1b , 4.7, 4.5, 4.6. These graphs are similar to the analytical results shown in Fig. 2.1a. In fact, the difference of the analytical and numerical results are of the order of the magnitude of the small parameter of the analytical theory (d_e/L). Due to the increasing density of the instability zones, very high resolution is required

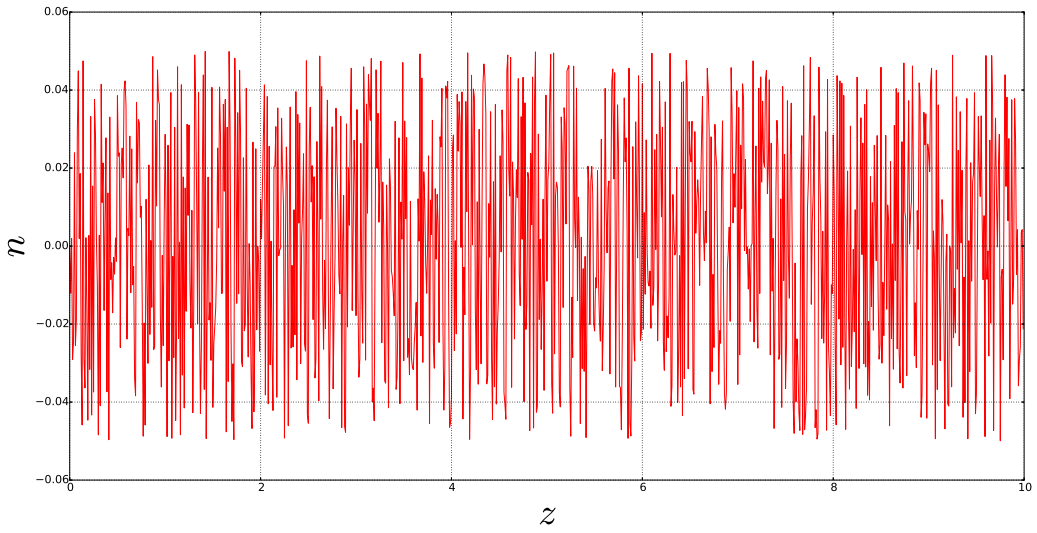

Figure 4.1: Example of random density initial conditions.

to recover the singular part ($v_0 \to 0$) of the analytical solution.

From the theory we know that instability will not occur in quasi-neutral case. In other words, charge separation is crucial for the instability to occur. Because in the long system charge separation is less prominent, we can expect decrease of instability growth rate with system length. This is confirmed by simulations for $L = 5$ (Fig. 4.7), $L = 10$ (Fig. 4.5) and $L = 15$ (Fig. 4.6).

In the regime when the length of the system is much smaller than the Debye length ($L \sim 0.1 d_e$), the difference between analytical solution of strong dispersion approximation and numerical solution was less than few percent. This comparison is shown in Fig. 2.2.

4.1 The form of unstable eigenfunctions

The number of zeros of unstable spatial eigenfunctions of density, velocity and electrostatic potential correlate with the zone number (2.26) and in strong dispersion case is defined by the value of the α parameter. In more general case, the stability of the system is governed by two parameters (v_0, L). However in general case the number of zeros correlates with a number of zone as well, examples of eigenfunctions are shown in Fig. 4.8.

In aperiodic zones (where real part of frequency is zero), the number of nodes does not change during the time evolution. In oscillatory zones, some nodes disappear at later times

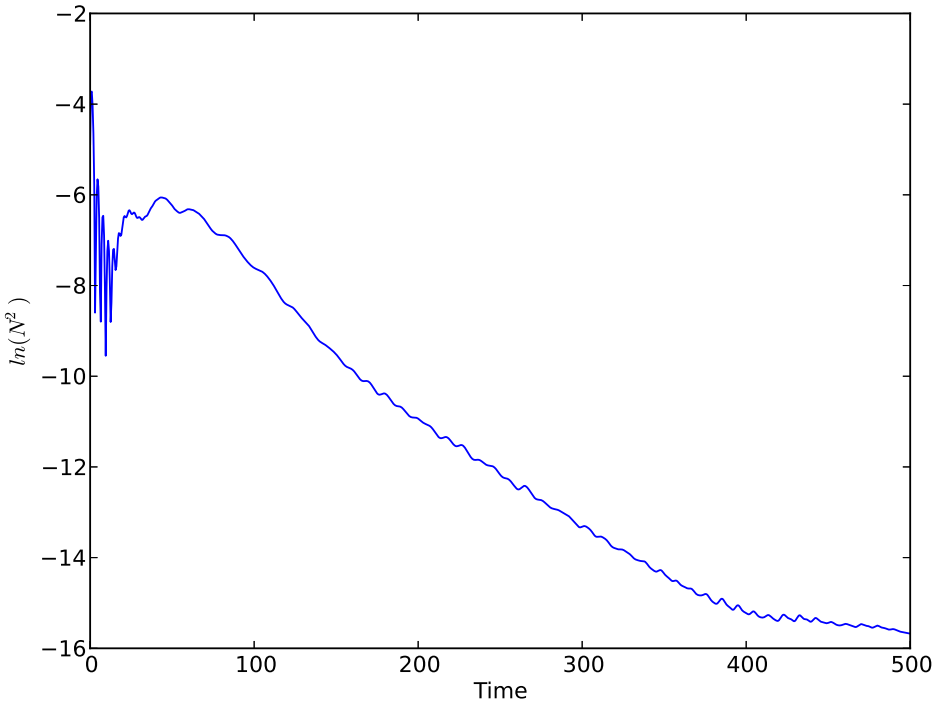

Figure 4.2: Evolution example of $\ln(N^2)$ in stable case.

as shown in Fig. 4.8d.

4.2 The evolution of unstable eigenfunctions

In weakly dispersive case ($kd_e \ll 1$), the addition of the Doppler shift due to the ion flow velocity results in the main order modification for the propagating modes velocities

$$v_{1,2} = v_0 \pm c_s, \tag{4.3}$$

which correspond to the one pair of the of the roots of Eq. (2.7). Two other roots describe the slow dispersion effects. We have chosen very long system ($L = 1000d_e$) so the dispersion is weak and two wave packets are well separated. Gaussian function localized in the middle of the system was chosen as an initial condition, Fig. 4.9a. Fig. 4.9b shows that the Gaussian peak separated into two wave packets moving in opposite directions with velocities $v_{1,2}$ from Eq. (4.3). The right wave packet meets the wall at the right and passes through the wall

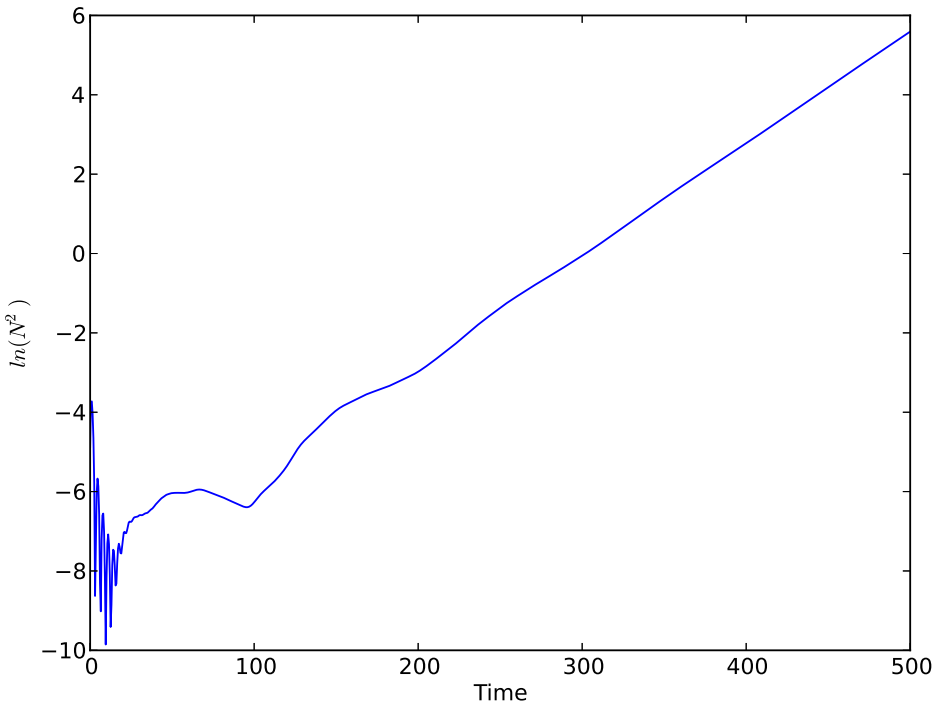

Figure 4.3: Evolution example of $\ln(N^2)$ in case of aperiodic instability.

with almost no reflection, as shown in Figs. 4.9c and 4.9d. Instability occurs when the slow wave packet meets the left wall (with Dirichlet boundary conditions for all variables) and is reflected, Fig. 4.9e. At a later time, the reflected wave and dispersion tail overlap forming an unstable eigenfunction, Fig 4.9e.

In strong dispersion case the equation (1.9) implies that oscillations with the ion plasma frequency will occur. The short system was chosen ($L = 0.1d_e$) to demonstrate this regime. Initial condition was chosen in the form of the Gaussian function localized in the middle. The evolution is shown in Figs. 4.10. First frame is an initial Gaussian peak which travels with the velocity of the ion flow (v_0); at the same time another peak arises from the left border and starts to travel with same velocity. Note that in case of strong dispersion, the ion sound phase velocity is much reduced, $\omega/k < c_s$. When the initial Gaussian peak meets the right boundary (which has no boundary conditions except the one for electrostatic potential) it passes through, while another peak starts to transform to unstable eigenfunction at the left boundary.

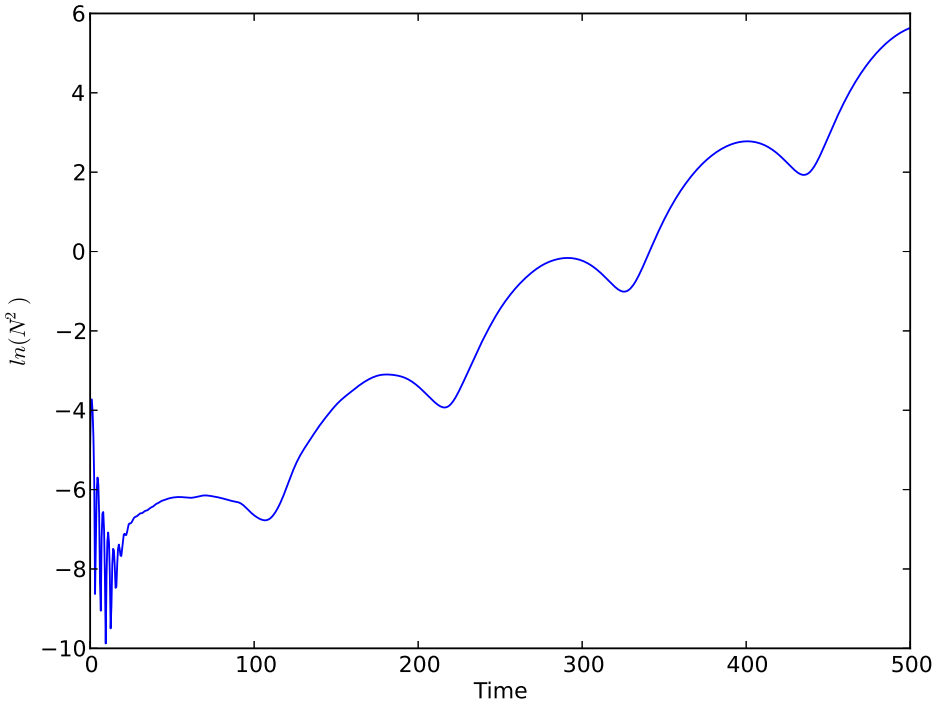

Figure 4.4: Evolution example of $\ln(N^2)$ in case of periodic instability.

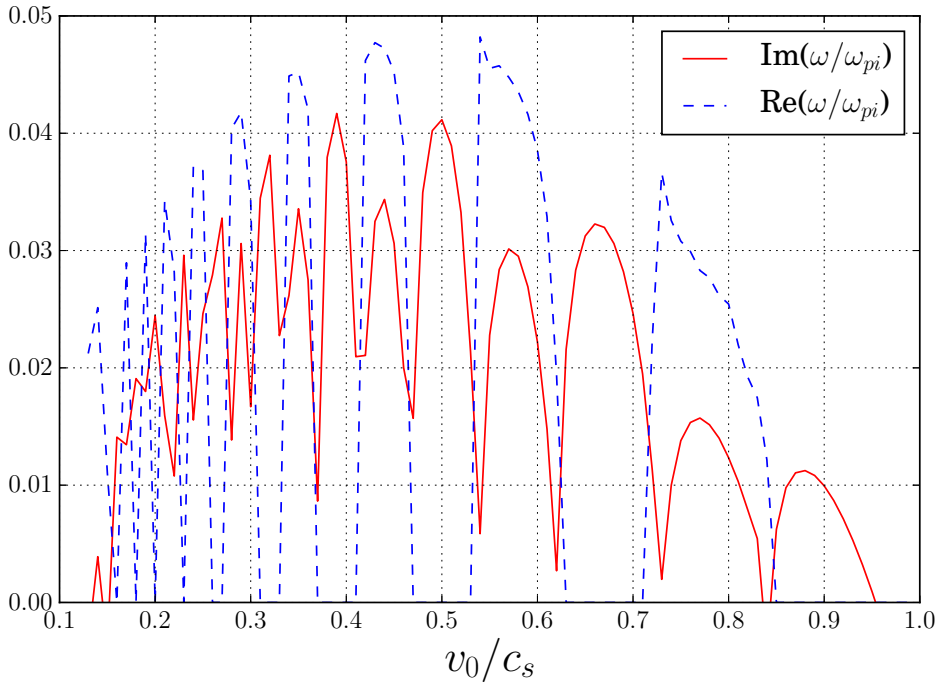

Figure 4.5: Alternating oscillatory ($\Re(\omega) \neq 0$) and aperiodic ($\Re(\omega) = 0$) instabilities zones in the intermediate system length $L = 10$; numerical simulations results.

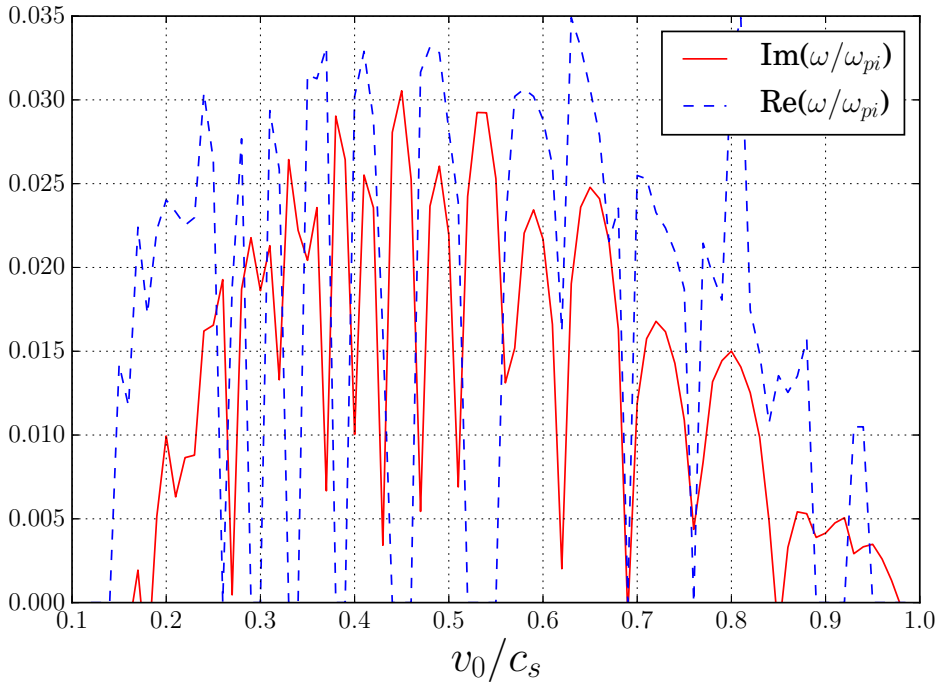

Figure 4.6: Alternating oscillatory ($\Re(\omega) \neq 0$) and aperiodic ($\Re(\omega) = 0$) instabilities zones in the intermediate system length $L = 15$; numerical simulations results.

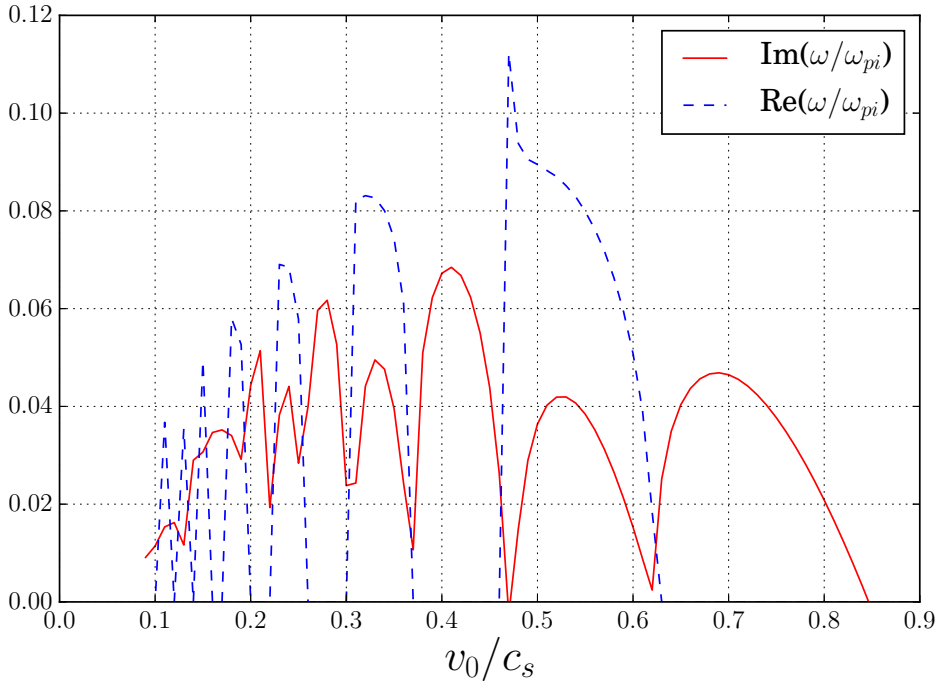

Figure 4.7: Alternating oscillatory ($\Re(\omega) \neq 0$) and aperiodic ($\Re(\omega) = 0$) instabilities zones in the intermediate system length $L = 5$; numerical simulations results.

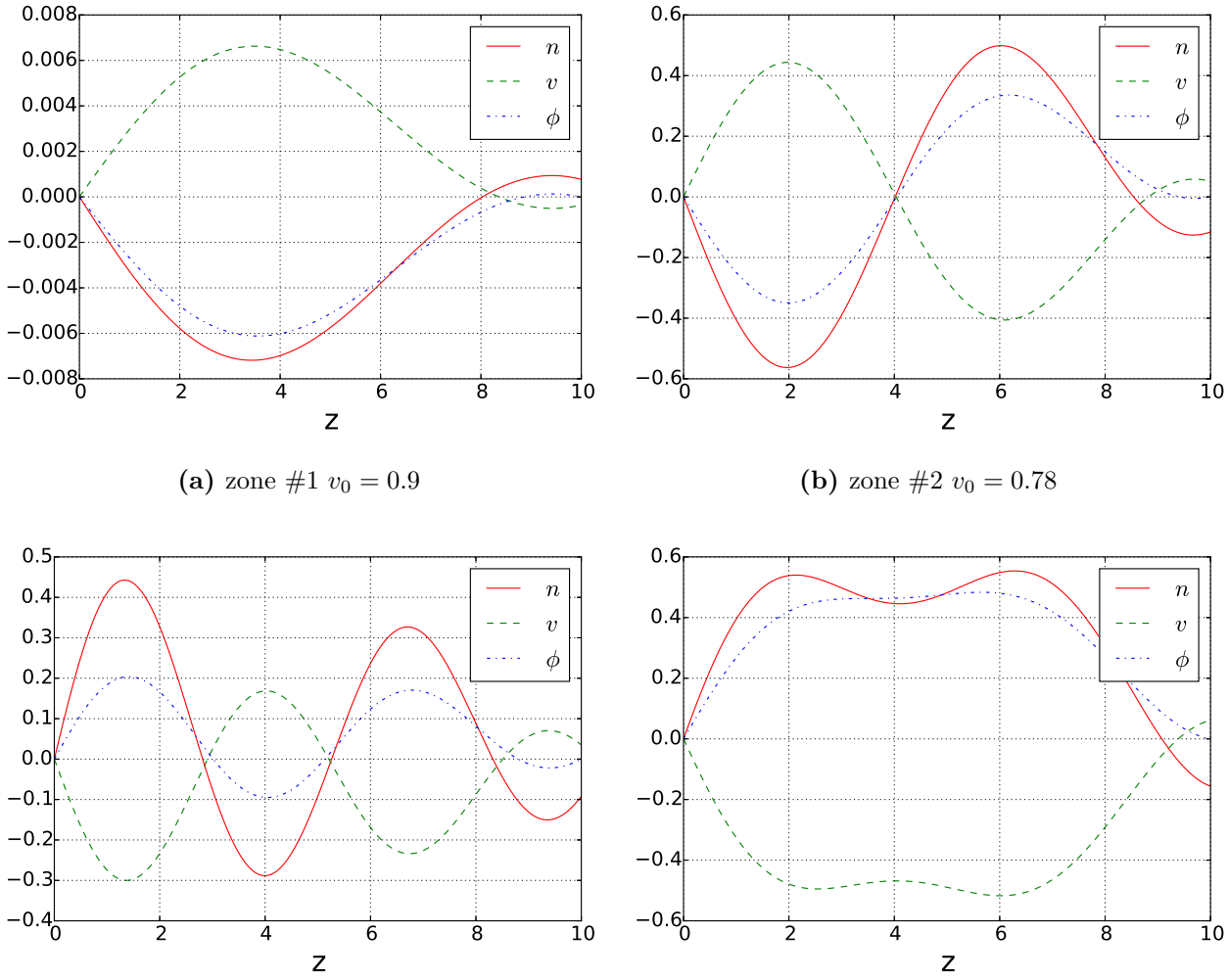

(a) zone #1 $v_0 = 0.9$

(b) zone #2 $v_0 = 0.78$

(c) zone #3 $v_0 = 0.65$

(d) zone #2 $v_0 = 0.78$

Figure 4.8: Unstable spatial eigenfunctions of density, velocity and electrostatic potential for $L = 10$, for different instability zones from Fig. 2.1. Zone numbers in Fig. 2.1 are counted from the right, with the right outermost aperiodic zone as #1. The last figure (d) shows temporal decreasing of nodes number due to oscillation.

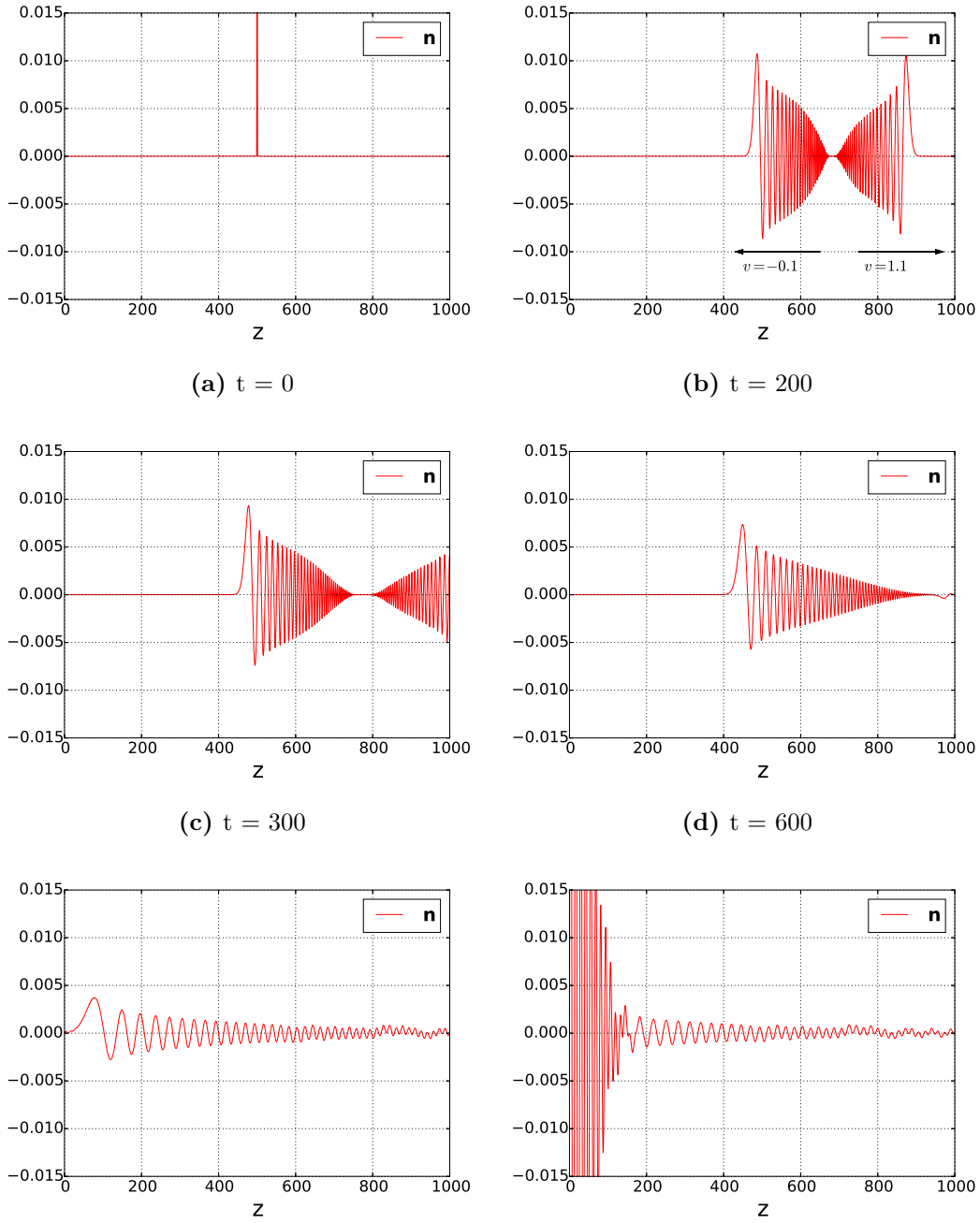

(a) t = 0

(b) t = 200

(c) t = 300

(d) t = 600

(e) t = 4400

(f) t = 5100

Figure 4.9: Evolution of the initial Gaussian pulse in the weak dispersion case: (a) initial condition; (b) initial perturbation splits into two traveling wave packets, the one traveling to the right with $v_0 + c_s = 1.9$ and the one traveling to the left with $v_0 - c_s = -0.1$; (c) the right wave packet is passing through the right wall barely reflecting; (d) the beginning of the reflection of the left wave packet from the wall and forming of the unstable eigen-function.

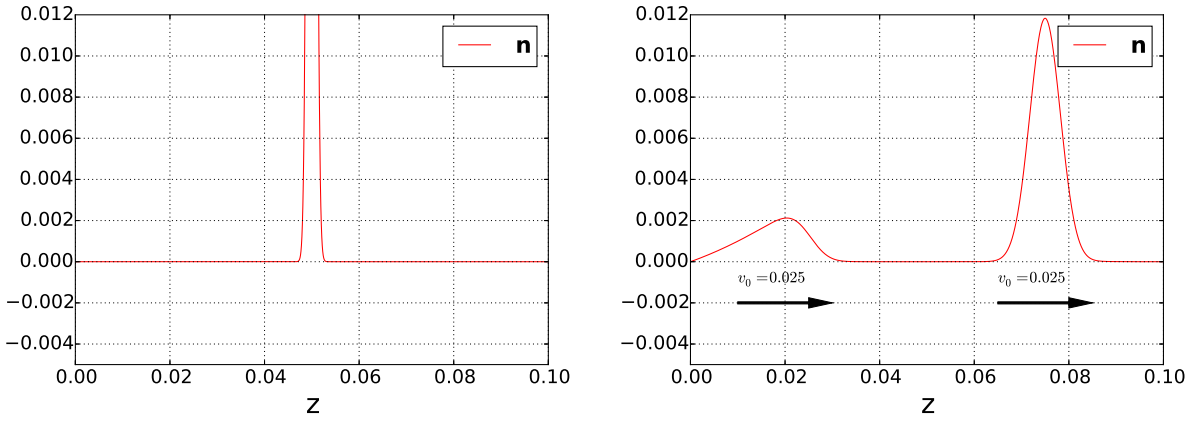

(a) t = 0 **(b)** t = 100

(c) t = 300 **(d)** t = 900

Figure 4.10: Dynamics in the strong dispersion case: (a) initial state; (b) the initial Gauss pulse travels with the velocity $v_0 = 0.025$ to the right, another pulse start to grow and travels to the right with the same velocity; (c) the initial pulse approaches the left boundary and the unstable eigen-function forms.

Chapter 5

Summary and conclusions

We have investigated the ion acoustic instability induced by the ion flow in a finite length system; the situation which is relevant to various plasma devices such as electric propulsion and emissive probe diagnostics. It was shown that the length of the system measured in units of the Debye length and ion flow velocity measured in units of the ion acoustic velocity are important parameters which control the instability. Analytical theory was developed and confirmed by the results of direct initial value numerical simulations. We have investigated the structure of the eigenfunctions in the unstable zones. It is shown that the order of the instability zone correlates with a number of nodes in the corresponding eigenfunction. Our numerical simulations show that the instability occurs as a result of the mode coupling mediated by the boundaries. The specific results of this work are:

1. Instability criteria, wave frequency and growth rates were obtained [23]. It was established that the criteria for the instability due to finite length effects are different from those for the standard kinetic ion sound instability [39].

2. It was shown that the instability occurs as a result of negative and positive energy modes coupling via wall boundary conditions.

3. A parallel fluid simulation code was developed. A good agreement between analytical and numerical results was demonstrated.

The excitation of large scale perturbations and soliton formation was observed in a number of experiments [40, 41]. Similar structures may be excited by the ion flow due to the mechanism identified in this work which is operative in systems of a finite length and in situations when the ion flow velocity is below the ion acoustic speed. The excitation of ion

sound waves in a finite length system was observed in numerical particle-in-cell simulations with emissive walls [42, 43]. The mechanism described in this work can also be relevant to the instabilities observed in double layer experiments [10, 44, 45].

5.1 Instability criteria

For long systems ($d_e \ll L$) the analytical dispersion equation (Eq. (2.19), Fig. 2.1) was obtained describing the aperiodic and oscillatory instability zones. The boundaries of the instabilities are defined by the condition (2.22). The instability criterion could also be written in the form

$$\frac{1}{1+\pi^2\frac{d_e^2}{L^2}} > \frac{v_0^2}{c_s^2}. \tag{5.1}$$

For short systems ($d_e \gg L$) the dispersion equation (Eq. (2.25), Fig. 2.2) was obtained in the form equivalent to the Pierce dispersion equation. In this case, the following instability criterion has been obtained

$$L\omega_{pi}/\pi > v_0. \tag{5.2}$$

The instability mechanism in a finite length system is different from the kinetic ion sound instability [39] in infinite plasmas. The dispersion equation for the latter can be written in the form

$$1 + \frac{\omega_{pi}^2}{k^2c_s^2} - \frac{\omega_{pi}^2}{\omega - kv_0} + i\sqrt{\frac{\pi}{2}\frac{m_e}{m_i}}\frac{\omega_{pi}^2\omega}{k^3c_s^3} = 0. \tag{5.3}$$

Treating $\epsilon = \sqrt{\frac{\pi}{2}\frac{m_e}{m_i}}$ as a small parameter, one obtains the growth rate

$$\gamma = \frac{\epsilon k c_s}{2(1+k^2d_e^2)^2}\left(-1 \pm \frac{v_0}{c_s}\sqrt{1+k^2d_e^2}\right). \tag{5.4}$$

The instability condition has a form

$$\frac{1}{1+k^2d_e^2} < \frac{v_0^2}{c_s^2}, \tag{5.5}$$

which is complementary to the condition (5.1).

5.2 Instability mechanism

Ion sound waves on the background of the equilibrium ion flow are described by Eqs. (2.1). For infinite length system (periodic boundary conditions), those equations result in the dielectric permittivity:

$$\varepsilon(\omega, k) = 1 + \frac{1}{k^2 d_e^2} - \frac{\omega_{pi}^2}{(\omega - k v_0)^2}, \tag{5.6}$$

The wave mode energy [46] corresponding to Eq. (5.6) is

$$\mathcal{E}(\omega, k) = \omega \frac{\partial \varepsilon}{\partial \omega} |k\phi|^2 = \frac{2k^2 \phi^2 \omega \omega_{pi}^2}{(\omega - k v_0)^3}, \tag{5.7}$$

It follows that the Doppler shift due to the ion flow results in negative energy perturbations for $\omega < k v_0$. Coupling of negative and positive energy modes results in reactive instabilities [47, 48]. In our case, the mode coupling occurs due to boundary conditions on the left wall as illustrated in Fig. 5.1. In Fig. 5.1a and 5.1b traveling wave packet arrives at the left boundary and starts forming the reflected wave. Further interaction of the reflected and original waves forms an unstable mode with an increasing (in time) amplitude as is shown in Figs. 5.1c and 5.1d.

The right boundary (with impinging ion flow), where only the potential is fixed, produces very little reflection, so that the reflected wave amplitude is much smaller than that of the incident wave (note the different scale in Fig.5.2c). There is no instability for the reflection from such a boundary as is illustrated in Fig. 5.2.

5.3 Parallel fluid simulations

Our system consists of different types of equations, thus, we have to use various approaches to allow simple generalization for nonlinear case and straightforward parallelization.
The implicit form of the initial value problem (3.1) suggests to make the inversion of Poisson equation (3.1c) at every time step. A number of different methods were used: calculation of the explicit integral, simple shooting method, relaxation and multiple shooting meth-

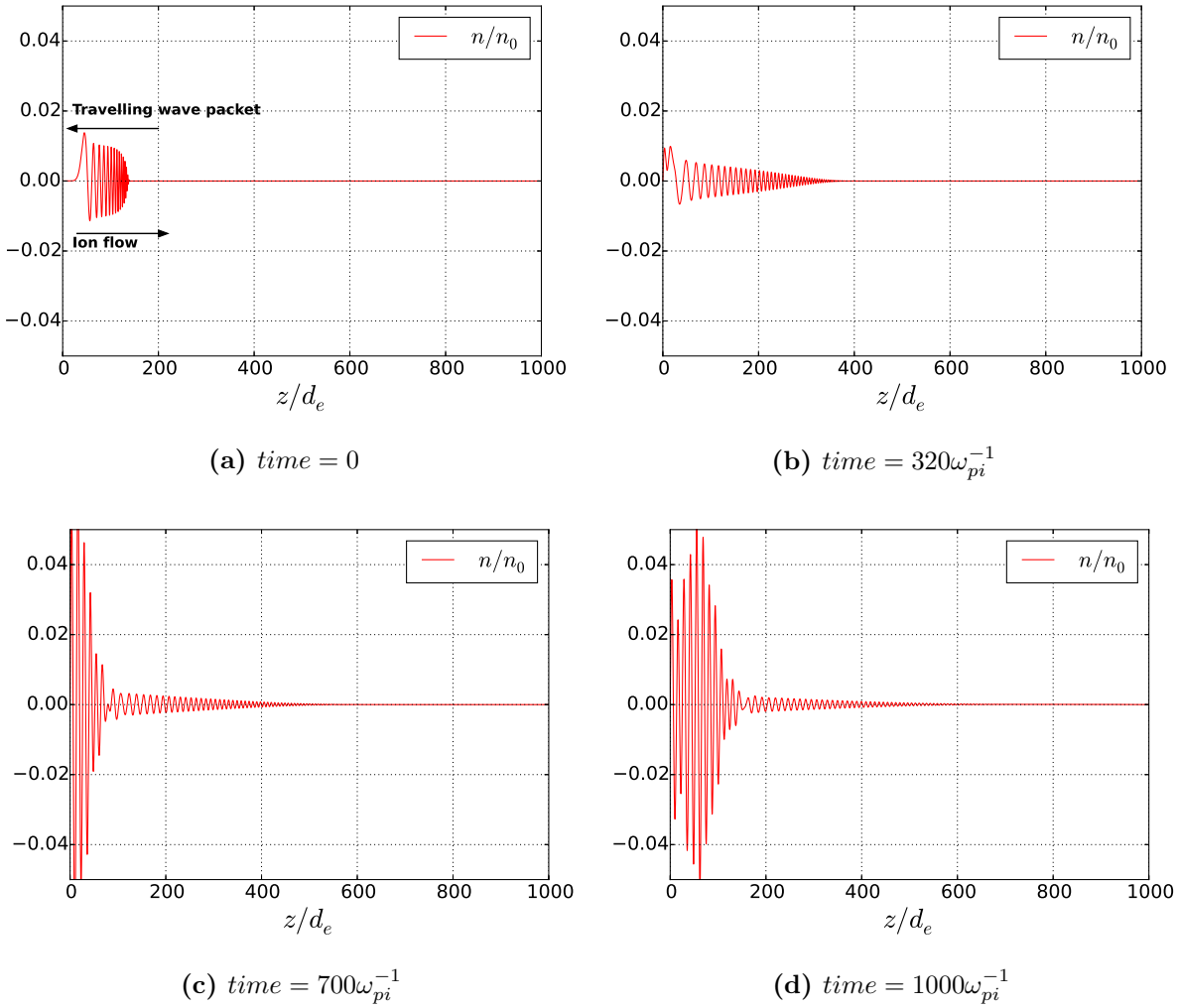

(a) $time = 0$ **(b)** $time = 320\omega_{pi}^{-1}$

(c) $time = 700\omega_{pi}^{-1}$ **(d)** $time = 1000\omega_{pi}^{-1}$

Figure 5.1: Formation of unstable eigenfunction due to reflection of the wave packet from the emitting boundary on the left.

ods. It was found that the multiple shooting method works better than the other methods. The multiple shooting method is relatively fast (for example in comparison with straightforward integral evaluation), easy to parallelize (comparing to relaxation methods) and has a straightforward generalization for the nonlinear case. Then, the conservative pair of equations (continuity and Euler equations) in system (3.1) was solved with different approaches. The fact that in our system the waves propagate in opposite directions produces a restriction for finite difference schemes. For example, a simple upwind scheme will be unconditionally unstable. To solve this issue, MacCormac, Lax–Friedrichs, and Godunov methods were tested. We have found that only the Godunov scheme proved to be useful, since MacCormac

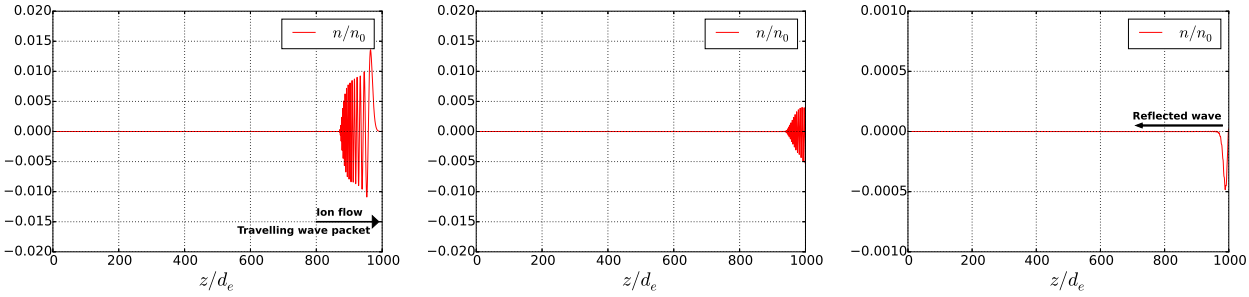

(a) $time = 0$ **(b)** $time = 70\omega_{pi}^{-1}$ **(c)** $time = 140\omega_{pi}^{-1}$

Figure 5.2: Reflection from the boundary with free density and velocity perturbations (on the right).

method showed oscillatory behavior while Lax–Friedrichs method has big artificial viscosity. Even though Godunov is only first order method, it leaves on open opportunity for high order generalization, for example, with WENO algorithm [49] which looks very promising for this problem.

The parallelization with the most common paradigms of shared and distributed memory were done. The well known libraries OpenMP and MPI were chosen correspondingly. The time benchmark tests for both version of the code were done and we can conclude that both approaches could significantly improve elapsed times. It is hard to conclude which method is the best because the speedup depends on the type of the hardware in use. So if one has limited number of cores and fast interconnect speed between them it is wise to use OpenMP, however if one has large number of processors available, the MPI will suit better.

Bibliography

[1] A. A. Galeev and R. Z. Sagdeev. Nonlinear plasma theory. In M.A. Leontovich, editor, *Reviews of Plasma Physics*, volume 7. Consultants Bureau, New York, 1979.

[2] J. Vranjes. New features of ion acoustic waves in inhomogeneous and permeating plasmas. *Astronomy & Astrophysics*, 554:A90, 2013.

[3] F. Skiff, G. Bachet, and F. Doveil. Ion dynamics in nonlinear electrostatic structures. *Physics of Plasmas*, 8(7):3139–3142, 2001.

[4] J. A. Wesson, A. Sykes, and H. R. Lewis. Ion-sound instability. *Plasma Physics*, 15(1):49, 1973.

[5] R. T. Farouki, M. Dalvie, and L. F. Pavarino. Boundary-condition refinement of the Child-Langmuir law for collisionless dc plasma sheaths. *Journal of Applied Physics*, 68(12):6106–6116, 1990.

[6] A. Y. Ender, H. Kolinsky, V. I. Kuznetsov, and H. Schamel. Collective diode dynamics: an analytical approach. *Physics Reports*, 328(1):1 – 72, 2000.

[7] H. Schamel and S. Bujarbarua. Lagrangian description of ion dynamical effects in plasma diodes. *Physics of Fluids B: Plasma Physics*, 5(7):2278–2285, 1993.

[8] A. M. Keesee, E. E. Scime, C. Charles, A. Meige, and R. Boswell. The ion velocity distribution function in a current-free double layer. *Physics of Plasmas*, 12(9):093502, 2005.

[9] S. D. Baalrud and C. C. Hegna. Kinetic theory of the presheath and the Bohm criterion. *Plasma Sources Science & Technology*, 20(2):025013, 2011.

[10] C. Charles. A review of recent laboratory double layer experiments. *Plasma Sources Science and Technology*, 16(4):R1, 2007.

[11] J. C. Johnson, R. L. Merlino, and N. d'Angelo. Double layers formed by ion-beam injection in a double-plasma device. *Journal of Physics D: Applied Physics*, 22(10):1456, 1989.

[12] A. Kapulkin, E. Behar, and Y. Raitses. Ion beam instability in hall thrusters. In *33rd International Electric Propulsion Conference*, 2013.

[13] J. R. Pierce. Limiting stable current in electron beams in the presence of ions. *Journal of Applied Physics*, 15(10):721–726, 1944.

[14] J. R. Cary and D. S. Lemons. Unstable oscillatory Pierce modes of neutralized electron beams. *Journal of Applied Physics*, 53(4):3303–3304, 1982.

[15] S. Kuhn. The physics of bounded plasma systems (BPS's): Simulation and interpretation. *Contributions to Plasma Physics*, 34(4):495–538, 1994.

[16] T. L. Crystal and S. Kuhn. Particle simulations of the low$-\alpha$ Pierce diode. *Physics of Fluids*, 28(7):2116–2124, 1985.

[17] B. B. Godfrey. Oscillatory nonlinear electron flow in a Pierce diode. *Physics of Fluids*, 30(5):1553–1560, 1987.

[18] M. Hiroshi, H. Yokoyama, and D. Summers. Computer simulations of the chaotic dynamics of the Pierce beam-plasma system. *Physics of Plasmas*, 3(1):177–191, 1996.

[19] A. B. Mikhailovskii. *Theory of plasma instabilities*. Consultants Bureau, 1974.

[20] N. M. Riskin and D. I. Trubeckov. *Nonlinear waves (in Russian)*. Nauka. Fizmatlit., 2000.

[21] G. B. Whitham. *Linear and Nonlinear Waves*. Wiley-Interscience, Pasadena, California, 1999.

[22] M. A. Lieberman and A. J. Lichtenberg. *Principles of plasma discharges and materials processing*. John Wiley & Sons, Inc., 1994.

[23] O. Koshkarov, A. I. Smolyakov, I. D. Kaganovich, and V. I. Ilgisonis. Ion sound instability driven by the ion flows. *Physics of Plasmas*, 22(5):052113, 2015.

[24] H. Schamel. Lagrangian fluid description with simple applications in compressible plasma and gas dynamics. *Physics Reports - Review Section of Physics Letters*, 392(5):279–319, MAR 2004.

[25] D. M. Goebel and I. Katz. *Fundamentals of Electric Propulsion*. John Wiley & Sons, Inc., 2008.

[26] A. I. Morozov and V. V. Savelyev. Fundamentals of stationary plasma thruster theory. *Reviews of Plasma Physics*, 21:pp 203–391, 2000.

[27] E. Y. Choueiri. Plasma oscillations in Hall thrusters. *Physics of Plasmas (1994-present)*, 8(4):1411–1426, 2001.

[28] H. B. Keller. *Numerical Methods for Two-Point Boundary-Value Problems*. Society for Industrial Mathematics, 1991.

[29] R. Bulirsch J. Stoer. *Introduction to Numerical Analysis*. Springer, 2002.

[30] U. M. Ascher and S. Y. P. Chan. On parallel methods for boundary value ODEs. *Computing*, 46(1):1–17, 1991.

[31] J. R. Westlake. *A Handbook of Numerical Matrix Inversion and Solution of Linear Equations*. Wiley, 1968.

[32] R. J. LeVeque. *Finite Volume Methods for Hyperbolic Problems*. Cambridge University Press, Cambridge, New York, 2002.

[33] A. Harten, P. Lax, and B. Leer. On upstream differencing and godunov-type schemes for hyperbolic conservation laws. *SIAM Review*, 25(1):35–61, 1983.

[34] P. L. Roe. Approximate Riemann solvers, parameter vectors, and difference schemes. *Journal of Computational Physics*, 43(2):357 – 372, 1981.

[35] R. Courant, K. Friedrichs, and H. Lewy. Über die partiellen differenzengleichungen der mathematischen physik. *Mathematische Annalen*, 100(1):32–74, 1928.

[36] S. Vetter, Y. Aoyama, and J. Nakano. *Practical MPI Programming*. IBM Redbooks, 1999.

[37] R. W. Hockney and C. R. Jesshope. *Parallel Computers 2: Architecture, Programming, and Algorithms*. Bristol and Philadelphia: Adam Hilger, 1988.

[38] E. A. Lee. The problem with threads. Technical Report UCB/EECS-2006-1, EECS Department, University of California, Berkeley, Jan 2006.

[39] A. I. Akhiezer. *Plasma electrodynamics*. Pergamon Press, Oxford, 1975.

[40] K. E. Lonngren. Soliton experiments in plasmas. *Plasma Physics*, 25(9):943, 1983.

[41] A. Hirose, O. Ishihara, S. Watanabe, and H. Tanaca. Response of ion acoustic waves to an impulse. *Plasma Physics*, 20(11):1179, 1978.

[42] J. P. Sheehan, N. Hershkowitz, I. D. Kaganovich, H. H. Wang, Y. Raitses, E. V. Barnat, B. R. Weatherford, and D. Sydorenko. Kinetic theory of plasma sheaths surrounding electron-emitting surfaces. *Phys. Rev. Lett.*, 111:075002, Aug 2013.

[43] D. Sydorenko. *Private Communication*, 2014.

[44] C. Rapson, O. Grulke, K. Matyash, and T. Klinger. The effect of boundaries on the ion acoustic beam-plasma instability in experiment and simulation. *Physics of Plasmas (1994-present)*, 21(5):052103, 2014.

[45] A. Aanesland, C. Charles, M. A. Lieberman, and R. W. Boswell. Upstream ionization instability associated with a current-free double layer. *Phys. Rev. Lett.*, 97:075003, Aug 2006.

[46] B. B. Kadomtsev, A. B. Mikhailovskii, and A. V. Timofeev. Negative energy waves in dispersive media. *JETP*, 20(6):1517, June 1965.

[47] C. N. Lashmore-Davies. Negative energy waves. *Journal of Plasma Physics*, 71:101–109, 4 2005.

[48] M. V. Nezlin. *Physics of Intense Beams in Plasmas*. IOP Publishing, Bristol and Philadelphia, 1993.

[49] X. D. Liu, S. Osher, and T. Chan. Weighted essentially nonoscillatory schemes. *Journal of Computational Physics*, 115(1):200–212, NOV 1994.